

Natural land carbon dioxide exchanges in the ECMWF Integrated Forecasting System: Implementation and Offline validation

Souhail Boussetta¹, Gianpaolo Balsamo¹,
Anton Beljaars¹, Anna Agusti-Panareda¹,
Jean-Christophe Calvet², Cor Jacobs³,
Bart van den Hurk⁴, Pedro Viterbo⁵,
Sebastien Lafont², Emanuel Dutra¹,
Lionel Jarlan⁶, Manuela Balzarolo⁷,
Dario Papale⁷, Guido van der Werf⁸.

Research Department

¹ ECMWF, Reading, UK.

² Météo-France, CNRM, 42 Av. G. Coriolis, 31057 Toulouse Cedex, France.

³ Wageningen University, P.O. Box 9101, 6700 HB Wageningen, the Netherlands.

⁴ KNMI, P.O. Box 201, 3730 AE De Bilt, the Netherlands.

⁵ Instituto de Meteorologia, Lisbon, Portugal.

⁶ CESBIO, Toulouse, France and LMI TREMA/Programme SudMed Faculté des Sciences Semlalia, Université Cadi Ayyad, Maroc.

⁷ UNITUS, Via S.M.in Gradi n.4, 01100, Viterbo, Italy.

⁸ VU University, Faculty of Earth and Life Sciences, Amsterdam, the Netherlands.

May 2012

This paper has not been published and should be regarded as an Internal Report from ECMWF.

Permission to quote from it should be obtained from the ECMWF.



European Centre for Medium-Range Weather Forecasts
Europäisches Zentrum für mittelfristige Wettervorhersage
Centre européen pour les prévisions météorologiques à moyen

Series: ECMWF Technical Memoranda

A full list of ECMWF Publications can be found on our web site under:
<http://www.ecmwf.int/publications/>

Contact: library@ecmwf.int

© Copyright 2012

European Centre for Medium Range Weather Forecasts
Shinfield Park, Reading, Berkshire RG2 9AX, England

Literary and scientific copyrights belong to ECMWF and are reserved in all countries. This publication is not to be reprinted or translated in whole or in part without the written permission of the Director. Appropriate non-commercial use will normally be granted under the condition that reference is made to ECMWF.

The information within this publication is given in good faith and considered to be true, but ECMWF accepts no liability for error, omission and for loss or damage arising from its use.

Abstract

A carbon module has been added to the land surface model of the European Centre for Medium-Range Weather Forecasts (ECMWF) in order to simulate the photosynthesis processes fixing carbon dioxide into the biomass (the gross primary production) and the release of carbon dioxide via land biogenic processes (ecosystem respiration). This land carbon parameterization, integrated with the Hydrology-Tiled ECMWF Scheme for Surface Exchange over Land (HTESSEL), benefits from accurate simulations of soil moisture and introduces the capability of interacting with atmospheric carbon transport models by providing a biospheric CO₂ flux (the Net Ecosystem Exchange NEE) as surface boundary condition.

A description of the new carbon-based land surface scheme is provided here, together with its optimization and extensive verification based on field site experiments representing different types of vegetation and climate regimes. In areas where field-sites observations are not available, inter-comparison with well established and widely used NEE products are presented and discussed. The key features and the limitations of the model are evaluated in offline simulations driven by realistic meteorological forcing. In addition, global land surface carbon fluxes are compared with similar outputs from other state-of-the-art carbon models both in offline and in atmospheric-coupled simulations within a global transport model, showing an improved description of the interannual variability of atmospheric CO₂ concentrations.

1 Introduction

The role of the surface processes and their coupling with the atmosphere is crucial for weather and climate modelling. The land surface influences the partitioning of energy, mass and momentum fluxes which in turn affects the atmosphere. Various studies with numerical weather prediction (NWP) and climate models, at different spatial and temporal scales have shown that an improved land surface representation does increase the skills of weather forecasting (Betts et al., 1996, Beljaars et al., 1999, Boussetta et al., 2008, Koster et al., 2010). The vegetation layer, via its impact on radiation, wind, rainfall interception and transpiration, plays an important role in the surface-atmosphere exchanges, and therefore an accurate representation of the processes driven by vegetation is essential in Earth System Models (ESM). As a fundamental component of ESM, many Land Surface Models (LSMs) have recently introduced carbon and nitrogen modules to enable a more realistic representation of the coupling between energy, water and carbon cycles (Baker et al., 2003, Bonan et al., 2010, Clark et al., 2011). Modelling of the complex interaction and feedback between vegetation and the atmosphere can also help to improve the understanding of the Earth system. The introduction of a more realistic representation of the vegetation cycle allows to account for the reciprocal feedback with the atmosphere from the seasonal (Boussetta et al., 2011) to the interannual time scales (Cox et al., 2000, Van den Hurk et al., 2003b).

Furthermore, the description of the carbon cycle (with photosynthesis and respiration as its main components) enlarges the modelling applications, as the simulated ecosystem fluxes can be included in atmospheric transport models either in a coupled or an offline configuration and be relevant for atmospheric data assimilation (Engelen et al., 2009). For the computation of the plant transpiration, most of the operational LSMs use either the Jarvis type approach (Jarvis, 1976) or a plant physiological approach (Farquhar and Sharkey, 1982, Goudriaan et al., 1985, Ball et al., 1987, Collatz et al., 1992) to estimate the stomatal conductance (g_s). The basic assumption in the Jarvis-approach is that the different environmental factors (soil moisture, temperature, humidity, solar radiation, CO₂)

have a mutually independent impact on gs that can be parameterized as a simple product of functions representing these factors. The plant physiological approach is based on the fact that CO_2 taken up for photosynthesis (An) largely uses the same pathway as water transpired from the plants: the stomata. By linking the plant transpiration flux to An through gs , interactions between the environmental factors that affect gs can be taken into account as well.

In this study, the ECMWF operational land surface scheme HTESSEL (Balsamo et al., 2011) is coupled with such a so-called photosynthesis-conductance (A-gs) model. The A-gs model is a modified version of the Jacobs (1994) model, taking into account the effects of soil water stress on the photosynthesis and canopy resistance (Calvet et al., 1998 and 2000). The A-gs model is a semi-empirical physiological model linking the leaf photosynthesis rate, and thereby stomatal conductance to external, surface and atmospheric factors (solar radiation, CO_2 concentration, air temperature, air humidity and soil moisture). In order to obtain the CO_2 balance at the ecosystem scale, the A-gs model is coupled to an ecosystem respiration module with a dependency on soil moisture and surface temperature. The latter module is modified to take into account cold region and snow pack effects on soil respiration.

In this paper we discuss the benefits of this new development in the ECMWF LSM model, describe the optimization of some of the parameters and evaluate the model by comparing to fluxtower observations, global land CO_2 flux products and atmospheric budgets. The starting point HTESSEL incorporates several years of parameterization developments (Viterbo and Beljaars, 1995, Viterbo et al., 1999, van den Hurk and Viterbo, 2003a, Balsamo et al., 2009, Dutra et al., 2010, Boussetta et al., 2011, Balsamo et al., 2011). This scheme, has been updated with photosynthesis and carbon dioxide emission modules. A detailed technical description of HTESSEL is provided in the ECMWF Integrated Forecast System (IFS) documentation (2011).

The carbon model described in this paper is fairly simple and although it describes the main responses of ecosystem scale CO_2 fluxes to environmental parameters like temperature, humidity, radiation, soil moisture, and leaf area, it does not have a land surface carbon pool as generally included in climate models. To represent effects of the soil carbon pool, a dependency on prescribed vegetation types and cover is adopted. As such the model is suitable for monitoring applications within the NWP environment where relevant prognostic variables are kept under control by data assimilation or climatological datasets. Such a system is for instance applied to global re-analysis as ERA-Interim (e.g. Dee et al., 2011) and it provides an advanced analysis of atmospheric variables (e.g. Simmons et al. 2010) and soil moisture and surface temperature using a wide range of observations. It is well known that carbon fluxes respond to these variables (Goudriaan et al. 1985, Farquhar and Sahrkey 1982, Ball et al. 1987, Bonan et al. 2010), so it is expected that the carbon fluxes benefit from a high quality meteorological and hydrological forcing.

Two new land model versions are presented here: (i) a fully coupled version (labelled CTESSEL) in which the plant physiological approach (A-gs) is used to compute the stomatal conductance for water vapour transpiration, and (ii) an uncoupled version (labelled CHTESSEL) which includes the carbon module, but calculates evaporation using a stomatal conductance formulation based on the original Jarvis approach.

The Jarvis and A-gs parameterizations are described in sections 2 and 3 respectively. The flux tower field-sites from which observations were obtained and the model parameter calibration method are presented in section 4. Model evaluation is done in offline mode for various flux tower sites. Results are presented in section 5 for both the turbulent energy fluxes and the CO₂ fluxes with the CTESSEL and CHTESSEL model versions. Section 6 presents the conclusions of this study and discusses the implications of introducing vegetation dynamics in a global model.

2 The Jarvis model

The Jarvis-type approach is used in many land surface models for NWP due to its relatively straightforward formulation. Empirical stress functions (with values ranging between 0 and 1) depend on environmental conditions and are used to modulate a preset maximum stomatal conductance, that regulates the water vapour flux. One of the hypotheses behind this formulation is that the stress functions are independent from each other. In HTESSEL, the following formulation of the canopy conductance g_s is adopted:

$$g_s = g_{s,\max} LAI [f_1(R_s) f_2(\bar{\theta}) f_3(D_a)], \quad (1)$$

with $g_{s,\max}$ the vegetation type-dependant maximum stomatal conductance, LAI the leaf area index and f_1, f_2, f_3 , three stress functions expressing effects on g_s of shortwave radiation, soil moisture stress and atmospheric humidity deficit, respectively:

$$f_1(R_s) = \min \left[1, \frac{bR_s + c}{a(bR_s + 1)} \right], \quad (2)$$

where R_s is the downward short-wave radiation and a, b, c are empirical constants,

$$f_2(\bar{\theta}) = \begin{cases} 0 & , \quad \bar{\theta} < \theta_{pwp} \\ \frac{\bar{\theta} - \theta_{pwp}}{\theta_{cap} - \theta_{pwp}} & , \quad \theta_{pwp} \leq \bar{\theta} \leq \theta_{cap} \\ 0 & , \quad \bar{\theta} > \theta_{cap} \end{cases}, \quad (3)$$

with θ_{pwp} and θ_{cap} (dependent on soil type) representing soil moisture at permanent wilting point and at field capacity respectively and $\bar{\theta}$ a root density weighted average over the different soil layers of the unfrozen soil water.

$$f_3(D_a) = e^{-g_D D_a}. \quad (4)$$

In (Eq. 4), D_a is the atmospheric humidity deficit, and g_D is a vegetation type dependent coefficient. The details of HTESSEL and its parameter settings are given in Balsamo et al. (2009).

3 The photosynthesis based approach (A-gs)

The A-gs approach is based on plant physiological considerations and describes the plant photosynthesis process and its dependence on CO_2 , temperature and soil moisture. The stomatal conductance is active for regulating both water vapour and CO_2 fluxes. The gross CO_2 assimilation by the canopy A_g is calculated using a photosynthesis module following Goudriaan et al. (1985). The net assimilation A_n (i.e. the net flow of CO_2 through the stomata) is A_g minus the dark respiration R_d .

Once the net assimilation is known, g_s can be derived by Kirchhoff's resistance/conductance analogy (see Fig. 1) from the net flow of CO_2 through the stomata and the difference between the CO_2 concentration outside the leaves and the concentration in the intercellular cavities.

For the description of g_s , we follow a stepwise approach with: (i) the definition of the temperature dependent parameters, (ii), the radiation response, (iii) the calculation of the ratio between internal and external CO_2 concentration, (iv) the computation of stomatal conductance, (v) inclusion of the soil moisture response and (vi) the vertical integration over the canopy. The basics of the model are described by Jacobs (1994) and Jacobs et al. (1996). For the details of the current extended formulation we follow the publications by Calvet et al. (1998, 2004).

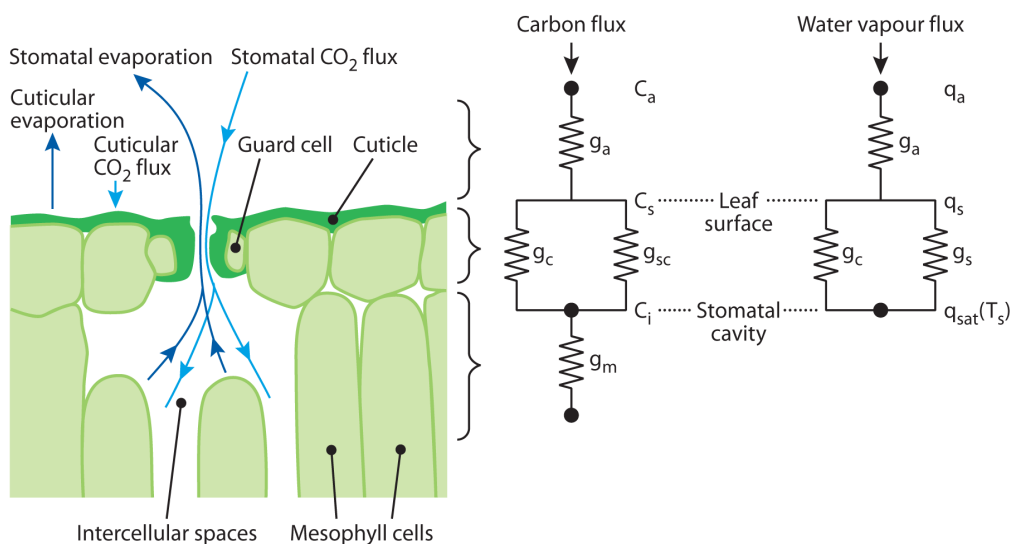


Figure 1: Schematic representation of a leaf with the resistance analogies for carbon and water vapour.

3.1 Temperature responses

There are several parameters in the photosynthesis model that are temperature dependent, namely the compensation point, the mesophyll conductance and the maximum photosynthetic capacity. The compensation point Γ is defined as the CO_2 concentration at which the net CO_2 assimilation of a fully lit leaf becomes zero. It can be measured in a laboratory by exposing plants to a variable CO_2

concentration. The mesophyll conductance g_m describes the transport of CO₂ from the substomatal cavities to the mesophyll cells where the carbon is fixed. It includes the representation of physical and chemical processes. The maximum photosynthetic capacity $A_{m,\max}$ is specified as an absolute upper limit to the photosynthesis rate in full sunlight and non-limiting CO₂ concentration.

The temperature dependence is described with so-called Q₁₀ functions, where Q₁₀ represents the proportional increase of a parameter for a 10 degree increase in temperature (Berry and Raison, 1982). For the compensation point the formulation is

$$\Gamma(T_s) = \Gamma(25^\circ) Q_{10\Gamma}^{(T_s - 25)/10}, \quad (5)$$

where $\Gamma(25^\circ)$ is the compensation point at 25° C, $Q_{10\Gamma}$ is the Q₁₀-constant and T_s is the leaf surface temperature. For g_m and $A_{m,\max}$, the temperature dependence is further adjusted by the inhibition functions after Collatz et al. (1992):

$$g_m(T_s) = \frac{g_m(25^\circ) Q_{10gm}^{(T_s - 25)/10}}{(1 + e^{0.3(T_{1gm} - T_s)}) (1 + e^{0.3(T_s - T_{2gm})})}, \quad (6)$$

$$A_{m,\max}(T_s) = \frac{A_{m,\max}(25^\circ) Q_{10Am,\max}^{(T_s - 25)/10}}{(1 + e^{0.3(T_{1Am,\max} - T_s)}) (1 + e^{0.3(T_s - T_{2Am,\max})})}, \quad (7)$$

where $Q_{10gm}, Q_{10Am,\max}, T_{1gm}, T_{2gm}, T_{1Am,\max}, T_{2Am,\max}$, are constants affecting the sensitivity to the plant surface temperature T_s . Parameter $g_m(25^\circ)$ depends on soil moisture stress and will be further described in section 3.5. Its unstressed value $g_m^*(25^\circ)$ is optimized here with the help of observations (see section 4). The constants in these functions are vegetation type dependent and are listed in Table 1 and 2.

3.2 Radiation and CO₂ response

For A_n , two regimes are distinguished: the radiation limiting regime and the CO₂ limiting regime (Goudriaan et al., 1985, Jacobs, 1994). In the radiation limiting regime with sufficient CO₂, A_n is controlled by the amount of photosynthetically active radiation (PAR) I_a

$$A_n = \varepsilon I_a - R_d, \quad (8)$$

where R_d is the dark respiration and where ε is the quantum efficiency expressed according to

$$\varepsilon = \varepsilon_o \frac{C_s - \Gamma}{C_s + 2\Gamma}. \quad (9)$$

Parameter ε_o is the maximum quantum use efficiency and C_s is the ambient CO₂ concentration at the leaf surface. At high radiation intensities, net assimilation saturates at a level A_m and becomes CO₂ limited according to $A_m = (C_i - \Gamma)g_m$ with C_i for the CO₂ concentration inside the leaf cavities (see below). An absolute limit to account for the maximum photosynthethic capacity of the leaves is further applied as follows

$$A_m = A_{m,\max} \left[1 - \exp\{-g_m(C_i - \Gamma)/A_{m,\max}\} \right]. \quad (10)$$

The radiation and CO₂ limiting regimes are combined via a smooth exponential transition function

$$A_n = (A_m + R_d) \left[1 - \exp\left(\frac{-\varepsilon I_a}{A_m + R_d}\right) \right] - R_d. \quad (11)$$

The autotrophic dark respiration is simply parameterised as

$$R_d = A_m / 9. \quad (12)$$

Type code	Vegetation type	R ₀ [mgCO ₂ /m ² /s]	g _m *(25) [mm/s]	g _c [mm/s]	Dmax [*] [kg/kg]	A _{m,max} (25) [mgCO ₂ /m ² /s]	f _o [*] [-]	Γ(25) [ppm]
1	Crops, mixed farming	0.100	1.3	0.15	Eq.22	2.20	0.85	42
2	Short grass	0.080	1.3	0.20	Eq.22	3.00	0.65	42
3	Evergreen needleleaf	0.360	0.8	0.20	0.124	2.20	Eq.26	42
4	Deciduous needleleaf	0.330	0.8	0.20	0.124	2.20	Eq.26	42
5	Deciduous broadleaf	0.280	1.4	0.00	0.109	1.83	Eq.26	42
6	Evergreen broadleaf	0.270	1.1	0.25	0.124	1.83	Eq.26	42
7	Tall grass	0.150	2.3	0.20	Eq.22	1.83	0.70	2.6
8	Desert	-	-	-	-	-	-	-
9	Tundra	0.360	2.0	0.25	Eq.22	3.00	0.95	42
10	Irrigated crops	0.096	1.4	0.25	Eq.22	1.83	0.92	42
11	Semidesert	0.019	1.0	0.25	Eq.22	1.83	0.80	42
12	Ice caps and glaciers	-	-	-	-	-	-	-
13	Bogs and marshes	0.270	0.5	0.25	Eq.22	1.83	0.96	42
14	Inland water	-	-	-	-	-	-	-
15	Ocean	-	-	-	-	-	-	-
16	Evergreen shrubs	0.110	0.9	0.15	Eq.22	1.83	0.72	2.6
17	Deciduous shrubs	0.080	1.9	0.20	Eq.22	1.83	0.96	42
18	Mixed forest-Wood	0.420	1.0	0.00	0.124	2.20	Eq.26	42
19	Interrupted forest	0.160	0.8	0.10	0.124	2.20	Eq.26	42
20	Water -land mixtures	0.270	1.0	0.25	Eq.22	1.83	0.95	42

Table 1: Parameter values as specified in the optimized CTESSEL model. The vegetation types are from the GLCC data base and used in the same way as in TESSEL (van den Hurk et al., 2000).

$Q_{10\Gamma}$	2	
Q_{10gm}	2	
$Q_{10Am,max}$	2	
$T_{1gm} (^{\circ}\text{C})$	5	13 for veg. types 7 and 16
$T_{1Am,max} (^{\circ}\text{C})$	8	13 for veg. types 7 and 16
$T_{2gm} (^{\circ}\text{C})$	36	
$T_{2Am,max} (^{\circ}\text{C})$	38	
a	2.381	5.323 for veg.types 7 and 16
b	-0.6103	-0.8923 for veg.types 7 and 16
$D_{max}^X (\text{g/kg})$	300	
$\varepsilon_o (\text{mg CO}_2/\text{J PAR})$	0.0142	0.0117 for vegetation types 7 and 16

Table 2: CTESSEL temperature response, quantum use efficiency and soil moisture stress parameters

3.3 The C_i / C_s ratio

In order to be able to derive stomatal conductance from the net assimilation, the CO_2 concentration inside the leaf cavities C_i needs to be known. Observations indicate that the ratio C_i / C_s is a rather conservative quantity for moist atmospheric conditions and that increasing humidity deficit exerts a strong stomatal control affecting this ratio. Therefore C_i / C_s is specified as a function of atmospheric moisture deficit D_s at the leaf surface.

$$\frac{C_i}{C_s} = f + (1-f) \frac{\Gamma}{C_s}, \quad (13)$$

where f is the coupling factor defined by:

$$f = f_o \left(1 - \frac{D_s}{D_{\max}} \right) + f_{\min} \frac{D_s}{D_{\max}}, \quad (14)$$

and f_o is the value of f at $D_s = 0 \text{ kg/kg}$, D_{\max} is the maximum saturation deficit and

$$f_{\min} = \frac{g_c}{g_c + g_m}. \quad (15)$$

The transport of CO_2 is maintained in the situation where $f = f_{\min}$ through the leaf cuticle or because of imperfect closure of the stomata. This process is represented by the cuticular conductance g_c .

3.4 Stomatal conductance

The first computation of the stomatal conductance for CO₂, g_{sc}^1 is achieved by dividing net assimilation by the difference between CO₂ concentration in and outside the leaves. It is modified here to account for the limiting cases of very dry air and dark respiration:

$$g_{sc}^1 = \frac{A_n - A_{\min} \left(\frac{D_s}{D_{\max}} \frac{A_n + R_d}{A_m + R_d} \right) + R_d \left(1 - \frac{A_n + R_d}{A_m + R_d} \right)}{C_s - C_i} \quad (16)$$

where A_{\min} represents the residual photosynthesis rate (at full light intensity) associated with cuticular transfers when the stomata are closed because of a high specific humidity deficit:

$$A_{\min} = g_m (C_{\min} - \Gamma). \quad (17)$$

In this equation, C_{\min} is the value of C_i at maximum specific humidity deficit:

$$C_{\min} = \frac{g_c C_s + g_m \Gamma}{g_c + g_m}. \quad (18)$$

The diffusion of CO₂ through the stomatal openings interacts with that of water vapour and therefore stomatal conductance to CO₂ is corrected for this interaction by an iterative refinement:

$$g_{sc} = g_{sc}^1 + E \frac{M_a}{\rho_a M_v} \frac{C_s + C_i}{2(C_s - C_i)}, \quad (19)$$

where M_v and M_a are molecular masses of water vapour and air respectively, ρ_a is the air density and E is the leaf transpiration based on the previous guess of the stomatal conductance:

$$E = (1.6g_{sc}^1) D_s \rho_a \quad (20)$$

Finally, the stomatal conductance to water vapour g_s is given by:

$$g_s = 1.6g_{sc}. \quad (21)$$

The total conductance used by the transpiration scheme is $g_s + g_c$, where g_c is the vegetation type dependent cuticular conductance (Table 1).

3.5 Soil moisture stress response

Unlike other A-gs formulations for which the soil moisture stress response is directly applied to the gross assimilation A_g (Ronda et al., 2001) or the net assimilation A_n (Sala and Tenhunen, 1996), Calvet (2000) found that the soil moisture stress response is driven in a complex way through the mesophyll conductance g_m , the maximum specific humidity deficit tolerated by the vegetation D_{\max} , and the ratio C_i / C_s controlled by f . The soil moisture response behaves differently for high and low

vegetation. In CTESSEL and CHTESSEL the adopted soil moisture stress response follows the function described in Calvet et al. (2000, 2004) and is based on a meta-analysis of several herbaceous and woody vegetation types.

3.5.1 Low vegetation formulation

Calvet (2000) found that the mesophyll conductance g_m and the maximum atmospheric moisture deficit D_{\max} vary with soil moisture but that they remain correlated according to

$$\ln(g_m(25^\circ)) = a - b \ln(D_{\max}), \quad g_m(25^\circ) \text{ in } [\text{mm s}^{-1}] \text{ and } D_{\max} \text{ in } [\text{g kg}^{-1}] \quad (22)$$

Therefore this equation is used to derive D_{\max}^* (maximum saturation deficit without soil moisture stress) from the tabulated $g_m^*(25^\circ)$, where superscript * indicates optimal soil moisture conditions and a and b are tabulated empirical coefficients (Table 2). Then the soil moisture stress index f_2 (see Eq. 3) is applied to find D_{\max} in stressed conditions according to a bilinear function with a breakpoint at a critical soil moisture stress index f_{2c} :

$$D_{\max} = D_{\max}^X \frac{f_2}{f_{2c}} \quad \text{for } f_2 < f_{2c}, \quad (23a)$$

$$D_{\max} = D_{\max}^X + (D_{\max}^* - D_{\max}^X) \frac{f_2 - f_{2c}}{1 - f_{2c}} \quad \text{for } f_2 \geq f_{2c}, \quad (23b)$$

where D_{\max}^X is the maximum value of D_{\max} corresponding to f_{2c} . The resulting D_{\max} is substituted in (Eq. 22) to find $g_m(25^\circ)$.

3.5.2 High vegetation formulation

Observations show that $g_m(25^\circ)$ is well correlated with the coupling factor f_0 according to the following empirical expression (Calvet 2004):

$$\ln(g_m^*(25^\circ)) = 4.7 - 7.0 f_0^*, \quad g_m(25^\circ) \text{ in } [\text{mm s}^{-1}] \quad (24)$$

In this case (Eq. 24) is used to derive $g_m^*(25^\circ)$ from the value f_0^* as tabulated according to vegetation type (Table 1). Subsequently a soil moisture stress function is applied to find $g_m(25^\circ)$:

$$g_m(25^\circ) = g_m^N \frac{f_2}{f_{2c}} \quad \text{for } f_2 < f_{2c}, \quad (25a)$$

$$g_m(25^\circ) = g_m^N + (g_m^*(25^\circ) - g_m^N) \frac{f_2 - f_{2c}}{1 - f_{2c}} \quad \text{for } f_2 \geq f_{2c}, \quad (25b)$$

where g_m^N is the stressed value of g_m derived from the Calvet (2004) meta-analysis with the following empirical function:

$$\ln(g_m^N) = 2.8 - 7.0 f_0^* \quad , \quad g_m^N \text{ in } [\text{mm s}^{-1}] \quad (26a)$$

After computing $g_m(25^\circ)$ according to (Eq.25), the stressed value for f_0 is derived with

$$\ln(g_m(25^\circ)) = 2.8 - 7.0 f_0 \quad , \quad g_m(25^\circ) \text{ in } [\text{mm s}^{-1}] \quad (26b)$$

Further details on the soil stress parameterization can be found in Calvet et al. (2000 and 2004) and Voogt et al. (2006).

3.6 Vertical integration from leaf to canopy

The net CO₂ assimilation calculated at the leaf scale is upscaled to the canopy scale assuming that leaf parameters do not vary with height in the canopy, and that the attenuation of the incoming shortwave radiation in the canopy can be computed using a simple radiative extinction model. The incoming PAR above the vegetation ($I_a(h)$, with h the canopy height) is assumed to be 48% of the incoming shortwave radiation and then further attenuated in the canopy. The dependence of PAR on height z within the canopy is described by Roujean (1996) according to:

$$I_a(z) = I_a(h)(1 - K(z)), \quad (27)$$

where K is the extinction function given by:

$$K(z) = \delta(\mu_s)K_{df}(z) + (1 - \delta(\mu_s))K_{dr}(z). \quad (28)$$

$K_{df}(z)$ and $K_{dr}(z)$ are the extinction coefficients of diffuse and direct light, respectively:

$$K_{df}(z) = 1 - e^{\left(\frac{-0.8bLAI(h-z)}{h}\right)}, \quad (29)$$

$$K_{dr}(z) = 1 - e^{\left(\frac{-\frac{G}{\cos(\mu_s)} \frac{bLAI(h-z)}{h}}{h}\right)}, \quad (30)$$

where μ_s is the solar zenith angle and G is a parameter that describes the distribution of leaves (a spherical angular distribution is assumed with G=0.5), δ is the ratio of diffuse to total downward shortwave radiation at the top of the canopy, $LAI(h-z)$ is the cumulative leaf area index above height z and b is the foliage scattering coefficient given by:

$$b = 1 - \frac{1 - \sqrt{1 - \omega}}{1 + \sqrt{1 - \omega}}, \quad (31)$$

based on the leaf single scattering albedo ω (=0.2) for the solar spectrum corresponding to the PAR. Parameter δ is given by:

$$\delta(\mu_s) = \frac{0.25}{0.25 + \cos(\mu_s)}, \quad (32)$$

Assuming a homogeneous leaf vertical distribution, the integrated canopy net CO₂ assimilation, dark respiration and conductance can be written as:

$$A_{nl} = LAI \int_0^1 A_n d(z/h), \quad (33)$$

$$R_{dl} = LAI \int_0^1 R_d d(z/h), \quad (34)$$

$$g_{sl} = LAI \int_0^1 g_s d(z/h). \quad (35)$$

In the above equations, LAI is defined as the ratio of leaf area covering a unit of ground area (m² m⁻²).

The integrations are parameterized with a three-point Gaussian quadrature method following Goudriaan (1986):

$$A_{nl} = LAI \sum_{i=1}^3 W_i A_n(z_i), \quad (36)$$

$$R_{dl} = LAI \sum_{i=1}^3 W_i R_d(z_i), \quad (37)$$

$$g_{sl} = LAI \sum_{i=1}^3 W_i g_s(z_i), \quad (38)$$

where W_i and z_i are the Gauss weights and levels, respectively.

3.7 Leaf Area index estimation

The estimate of the Leaf Area Index is crucial for deriving the plant assimilation and its evolution, as it is the main indicator for the vegetation status. In this study a satellite observation-based climatology (also used in the operational IFS model) was considered for the representation of LAI. Additionally, LAI from a simple prognostic vegetation model based on nitrogen dilution which has the advantage over climatology to describe anomalies but not constrained by observations is being investigated for future usage within CTESSEL.

The satellite product (MOD15A2) is derived from the Moderate Resolution Imaging Spectroradiometer (MODIS) instrument on board of TERRA. It is produced daily for land surface at 1 km spatial resolution from MODIS spectral reflectance with a global coverage, and synthesized on an 8-day time interval based on simultaneously retrieved maximum Fraction of absorbed PAR (FPAR) in order to remove the atmospheric noise (Myneni et al., 2002).

The collection 5 of the product (released in 2008 available from February 2000 to present) is used in this study. To derive the climatological time series, 9 years of data (2000 -2008) were re-projected from the sinusoidal to a geographic regular lat/lion projection, spatially averaged to 1/12th degree resolution, then temporally smoothed, monthly averaged (Jarlén et al., 2008) and finally interpolated to

the IFS reduced Gaussian grid. The MODIS LAI products were analysed and validated in previous studies (Carrigues et al., 2008, MODIS Land team <http://landval.gsfc.nasa.gov/>). After a positive assessment within the IFS system (Boussetta et al., 2011), this product was adopted by ECMWF for operational use. As a first approach this climatology is tested within CTESSEL/CHTESSEL to drive the carbon flux module..

3.8 Soil respiration and ecosystem exchanges parameterization

In order to obtain the net exchange of CO₂ between the surface and atmosphere by a NWP model, soil respiration needs to be represented. Schemes relying on prognostic land carbon pools are less practical for NWP purposes owing to their difficulties to be initialized without a very long spin-up. In CTESSEL/CHTESSEL the CO₂ ecosystem respiration R_{eco} is split into two terms. The first is the autotrophic dark respiration R_{dl} (Eq. 37), while the second term $R_{soilstr}$ represents both heterotrophic respiration from the soil and autotrophic respiration from the above and below ground structural biomass. It is parameterized as a function of soil temperature, soil moisture, snow depth and vegetation type as:

$$R_{soilstr} = R_{eco} - R_{dl} = R_0(25)Q_{10Ro}^{\left(\frac{T_{soil}-25}{10}\right)} f_{sm} f_{sn}. \quad (39)$$

In this equation f_{sn} and f_{sm} are snow and soil moisture attenuation functions respectively defined as:

$$f_{sn} = 1 - C_{vs}(1 - e^{-\alpha z_{snow}}). \quad (40)$$

C_{vs} is the surface fraction covered by snow, α is a constant expressing the attenuation of the soil carbon emission within the snow pack and z_{snow} is the snow depth. The soil moisture stress function for soil respiration is defined following a study by Albergel et al. (2010) as:

$$f_{sm} = \frac{\bar{\theta}}{\theta_{cap}}. \quad (41)$$

In this case, given its variability with climate regimes, Q_{10Ro} is defined as a function of soil temperature after McGuire et al. (1992). The vegetation types are affecting the ecosystem respiration through a reference respiration at 25°C ($R_0(25)$) estimated by minimizing the root mean square errors between simulated and observed R_{eco} for each vegetation type (see section 4).

Finally, the relation between the gross primary production GPP , the net ecosystem exchange NEE and the respiration components ($R_{dl}, R_{soilstr}, R_{eco}$) are given by:

$$GPP = A_{nI} + R_{dl}, \quad (42)$$

$$NEE = A_{nI} - R_{soilstr} = GPP - R_{eco}. \quad (43)$$

4 Verification data and Parameter Calibration

4.1 Observation data

Available observational data for the years 2004 and 2006 from the Boreal Ecosystem Research and Monitoring Sites (BERMS) (Betts et al. 2006), the FLUXNET eddy-covariance network (Balocchi et al., 2001 and Balocchi et al., 2008) and the Coordinated Energy and water cycle Observations Project (CEOP) were used in this study.

For many years, BERMS has been providing high quality data especially useful for model evaluation and parameter optimization. The BERM sites used in this study consist of observations from 2 contrasting locations less than 100 km apart in Saskatchewan at the southern edge of the Canadian boreal forest (at about 54°N/105°W). The two locations are: the Old Aspen site (deciduous, open canopy, hazel under-story) and the Old Black Spruce site (evergreen needleleaf and boggy, moss under-story).

Number	Site	Network	Lat [°N]	Lon [°E]	Vegetation Type	Reference / PI
1	sk-oa	berms	53.63	-106.20	DBF	T. Andrew Black
2	sk-obs	berms	53.99	-105.12	ENF/WET	T. Andrew Black
3	brasilia	ceop	-15.93	-47.92	WSA/GRA/SH	Antonio Ocimar Manzi
4	manaus	ceop	-2.61	-60.21	EBF	Antonio Ocimar Manzi
5	at-neu	fluxnet	47.12	11.32	GRA	Wohlfahrt G., et al., (2008)
6	ca-mer	fluxnet	45.41	-75.52	WET	Lafleur, P.M., et al. (2003)
7	ca-qfo	fluxnet	49.69	-74.34	ENF	Bergeron, O., et al., (2007)
8	ca-sf1	fluxnet	54.49	-105.82	ENF	M.S. Mkhabela et al., (2009)
9	ca-sf2	fluxnet	54.25	-105.88	ENF	M.S. Mkhabela et al., (2009)
10	ch-oe1	fluxnet	47.29	7.73	GRA	Ammann C., et al., (2007)
11	fi-hyy	fluxnet	61.85	24.29	ENF	Timo Vesala
12	fr-hes	fluxnet	48.67	7.06	DBF	André Granier
13	fr-lbr	fluxnet	44.72	-0.77	ENF	Berbigier P., et al. (2001)
14	il-yat	fluxnet	31.34	35.05	ENF	Dan Yakir
15	it-amp	fluxnet	41.90	13.61	GRA	Riccardo Valentini
16	it-cpz	fluxnet	41.71	12.38	EBF	Dario Papale
17	it-mbo	fluxnet	46.02	11.05	GRA	Damiano Gianelle
18	it-ro1	fluxnet	42.41	11.93	DBF	Riccardo Valentini
19	it-ro2	fluxnet	42.39	11.92	DBF	Dario Papale
20	nl-ca1	fluxnet	51.97	4.93	GRA	Eddy Moore
21	nl-haa	fluxnet	52.00	4.81	GRA	Eddy Moore
22	nl-hor	fluxnet	52.03	5.07	GRA	Han Dolman

23	nl-loo	fluxnet	52.17	5.74	ENF	Eddy Moore
24	ru-fyo	fluxnet	56.46	32.92	ENF	Andrey Varlagin
25	ru-ha1	fluxnet	54.73	90.00	GRA	Belelli Marchesini
26	ru-ha3	fluxnet	54.70	89.08	GRA	Belelli Marchesini
27	se-sk2	fluxnet	60.13	17.84	ENF	Anders Lindroth
28	us-arm	fluxnet	36.61	-97.49	CRO	Fischer, M.L, et al. (2007)
29	us-bar	fluxnet	44.06	-71.29	DBF	Andrew Richardson
30	us-ha1	fluxnet	42.54	-72.17	DBF	Bill Munger
31	us-mms	fluxnet	39.32	-86.41	DBF	Danilo Dragoni
32	us-syv	fluxnet	46.24	-89.35	MF	Kenneth J. Davis
33	us-ton	fluxnet	38.43	-120.97	MF/WSA	Ma, S., et al. (2007)
34	us-var	fluxnet	38.41	-120.95	GRA	Ma, S., et al. (2007)

Table 3: List of sites used for the verification of the simulated fluxes, where the biome types are: deciduous broadleaf forest (DBF), evergreen broadleaf forest (EBF), deciduous needleleaf forest (DNF), evergreen needleleaf forest (ENF), mixed forest (MF), woody savannas (WSA), grasslands (GRA), crops (CRO), wetlands (WET)

As part of the CEOP program, reference sites observations from the Amazonian region, also belonging to the LBA experiments (the Large Scale Biosphere-Atmosphere Experiment in Amazonia) are available for scientific use. In this study, observations are taken from flux towers located within an evergreen broadleaf forest (Manaus) and a woody savannah region (Brasilia).

The FLUXNET data used are LaThuile in-situ observations (<http://www.fluxdata.org>), a dataset including 253 research sites belonging to the FLUXNET eddy covariance network. This dataset provides latent heat flux (LE), sensible heat flux (H) and net ecosystem exchange (NEE) at high temporal resolution (30 min to 60 min) and values for gross primary production (GPP) and ecosystem respiration (Reco) derived from halfhourly observed NEE following the partitioning method proposed in Reichstein et al. (2005). We only used observations flagged as high-quality data, without gap filling. As stated above, the observation sites used in this study cover a range of different climate and ecosystem zones mostly located at the midlatitudes (North America and Europe), with additional two tropical sites. Sites from high latitudes regions were not available to us (details are presented in Table 3). Optimization of a number of coefficients was performed using observations from the year 2006 and data from 2004 were used for verification.

4.2 Offline simulations

The Offline (or stand-alone) simulations offer a convenient framework for isolating the benefits and the deficiencies of a given land surface parameterization from any source of additional disturbance that may occur due to the surface-atmosphere interaction when running in coupled mode. In addition, in terms of computation cost, given the complexity of the coupling with the atmosphere, offline simulations are much cheaper (and thus faster) to run. In this study, offline runs were performed both at the global and point scales and all the land simulations were forced with 3-hourly meteorological data extracted from the ECMWF Era-Interim reanalysis (Dee et al., 2011), which covers the period from 1979 to present. These forcing data are gridded on a reduced Gaussian grid (N128) corresponding

to a resolution of 0.7° over the equator. The temperature, surface pressure, humidity and wind fields are instantaneous values and representative of the lowest model level corresponding to a height of 10m above the surface. The Incoming surface radiation in its long and short-wave components, the rainfall and snowfall are provided as 3-hourly accumulations. All these forcings were linearly interpolated in time to the land surface model timestep of 30 minutes.

For the global simulation (section 5.2), the land-use information has been derived from the GLCC data set at the same resolution as the forcing data. In the case of point simulations when performing the optimization procedure (section 4.3), the land-use information was set to correspond to the specific status of the site in order to ensure that the optimization is applied to the correct vegetation type. However, in the case of point simulations for validation (section 5.1), the vegetation type of the GLCC data was taken and no attempt was made to tune the derived vegetation characteristics to specific field site conditions, therefore these results should be indicative of the expected accuracy of a global model.

4.3 Optimization procedure

During its development, the A-gs model was initially designed and tested on a single field location (Jacobs et al., 1996), followed by an extension to regional and global domains (Calvet, 1998, Gibelin et al., 2006) using the ECOCLIMAP vegetation database (Masson et al., 2003). As in the previous HTESSEL model, CTESSEL and CHTESSEL use the Global Land Cover Characteristics (GLCC) data (Loveland et al., 2000) according to the Biosphere-Atmosphere Transfer Scheme (BATS) classification to assign dominant high and low vegetation types and associated fractional covers to each model grid box.

In this study, the model parameters were optimised by vegetation types in order to be compatible with the operational HTESSEL, and to accommodate the modifications brought to the model. In addition, stratifying the model parameters according to the 20 vegetation types of the BATS classification would allow to implicitly overcome the shortcoming of not explicitly representing the C3/C4 classes. Since GPP is computed independently from the ecosystem respiration (Reco) (Eq.43), and observational data are available for both GPP and Reco, the parameter optimization procedure was performed in two steps. First, the unstressed mesophyll conductance g_m^* used in the GPP calculation is estimated, and subsequently the reference respiration R_0 relevant to the simulation of Reco is computed by minimizing the root mean square error (rmse) between observed and simulated carbon fluxes (GPP for g_m^* and Reco for R_0). The available eddy covariance data were grouped by vegetation type and the observation period considered in the optimization is 2006 while year 2004 was used for the validation.

The optimization procedure is applied for each group of sites, allowing the considered parameters to vary within a fixed range of values chosen from the literature. Using this procedure, the optimized parameters for each vegetation type converged toward values yielding minimum errors with the observed fluxes. An illustrative example is shown in Figure 2 for the needle-leaf forest type where a minimum rmse is obtained between observed and simulated ecosystem respiration for $R_0=0.36$ [$\text{mgCO}_2 \text{ m}^{-2} \text{ s}^{-1}$], while the errors between observed and simulated GPP converge to an optimal value of $g_m^*=0.8[\text{mm/s}]$. The results of the optimized value for R_0 and g_m^* are presented in Table 1 together

with the other model parameters extracted from previous studies described in Calvet et al. (2000 and 2004) and White et al. (2000).

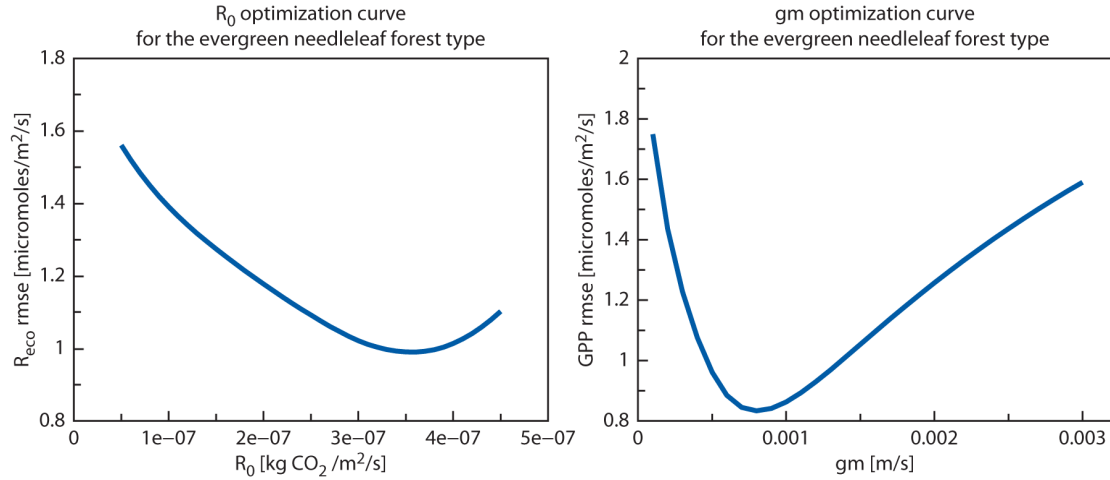


Figure 2: rmse of R_{eco} as a function of the reference respiration R_0 (left), and the rmse of GPP as a function of the mesophyl conductance \mathcal{G}_m^ (right). These curves apply to the evergreen needleleaf forest type. The minimum values of these curves have been selected as optimal parameters ie. $R_0=3.6 \cdot 10^{-7} [\text{kg CO}_2/\text{m}^2/\text{s}]$ and $\mathcal{G}_m^*=0.0008 [\text{m/s}]$.*

5 Results

To assess these new developments within the land surface scheme CTESSEL and its variant CHTESSEL, in-situ and global integrations of the model were performed. The in-situ simulations consisted of single point offline simulations over the available FLUXNET, BERMS and CEOP data covering various types of vegetation for the year 2004 which had the largest observation coverage of the available records (34 stations). Both the energy and the carbon cycles are evaluated. The global offline runs are compared with other state-of-the-art CO₂ products over a period of 6 years between 2003 and 2008. Finally, the CO₂ fluxes from CHTESSEL are used as boundary conditions in the global transport model of the Monitoring of Atmospheric Composition and Climate project (MACC), in order to evaluate the impact of simulated NEE on the atmospheric CO₂ concentrations.

5.1 In-situ simulations

Blyth et al. (2010) showed that a reasonable evaluation of the performance of a land surface model can be obtained by using data from 10 differing observation sites. In this study, results and scores of all the considered 34 stations covering various biomes and climate zones (Section 3) are presented, from which a selection of 6 stations representing different vegetation types is used to show time series for illustrative purposes.

5.1.1 Energy fluxes

Comparison between observed and simulated energy fluxes for all the considered stations allows the assessment of the performance of the two model versions (i.e. using the Jarvis-approach CHTESSEL

or using the A-gs approach CTESSEL) under similar conditions. Figure 3 shows the correlation of the two model versions against the eddy-covariance measurements of the 10-day average energy fluxes. Overall, both model versions (CTESSEL and CHTESSEL) show reasonable scores with high correlations (>0.8 on average) over all biomes except for the Manaus tropical station (Fig.3-c). Here the radiative forcing suffers from a known cloudiness bias over the ITCZ region (Dee et al., 2011). A slightly better skill in terms of bias and rmse of both latent and sensible heat fluxes was achieved with CTESSEL, using the photosynthetic-based A-gs formulation (Table 4).

In Figures 4 and 5 a comparison of the annual cycle of latent and sensible heat fluxes with in-situ observations is shown for both CTESSEL and CHTESSEL model versions for a selection of sites with different vegetation types. Both model versions perform reasonably well at the seasonal scale, with relatively small differences among them. This is an encouraging result given the fact that the Jarvis approach has benefited from a long experience of model-observation evaluation since it has been implemented in the operational model for many years already, whereas the A-gs did not benefit of such operational evaluation. The mean net radiation scores are hardly distinguishable between the two model versions, nevertheless, being of opposite signs, the bias in latent and sensible heat fluxes when using CTESSEL is smaller than that of CHTESSEL (table 4).

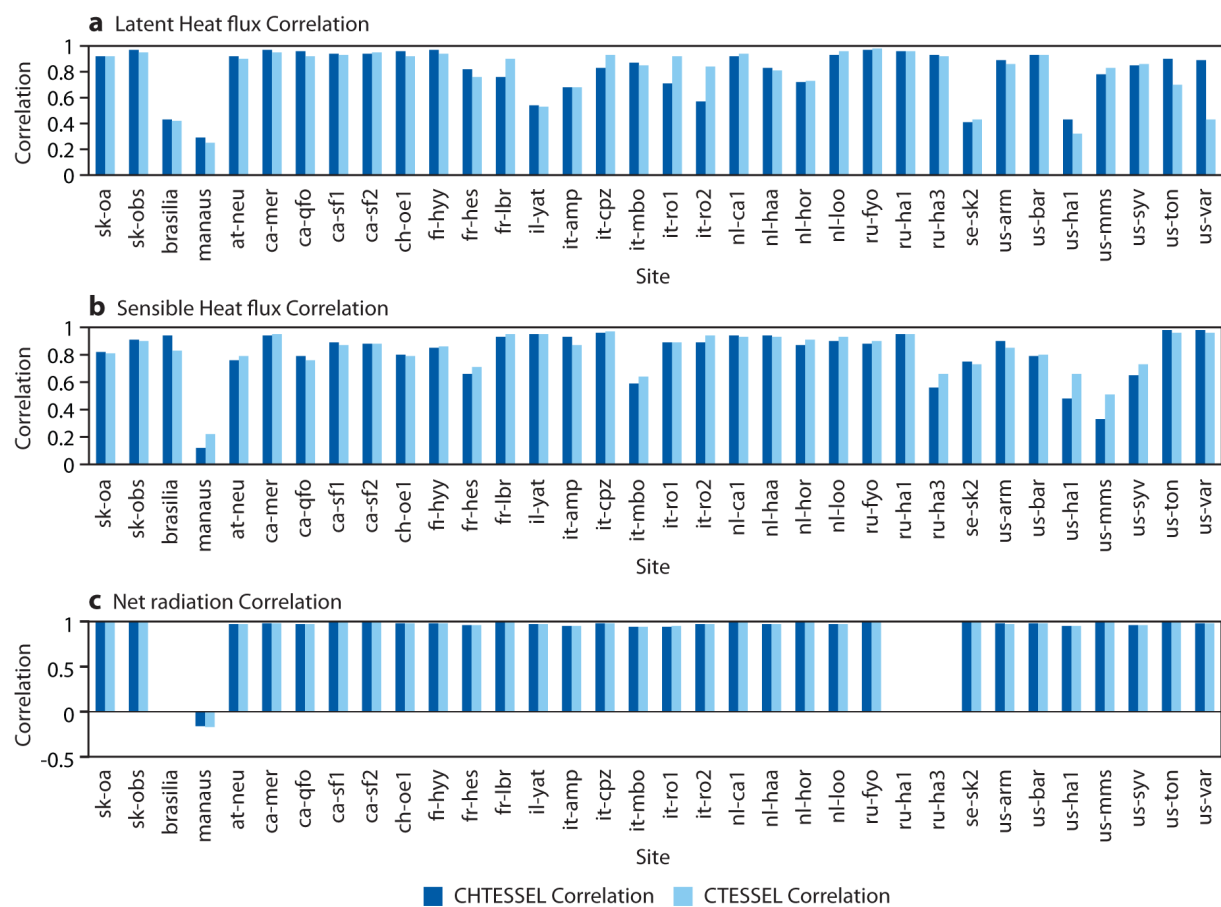


Figure 3: Correlation of the simulated energy fluxes with the eddy-covariance observation over the 34 sites. Dark blue bars are for CHTESSEL runs and light blue bars are for the CTESSEL results. (a) Latent heat flux, (b) Sensible heat flux and (c) Net radiation. Blank space in the graph refers to no or incomplete observations at the station for that parameter.

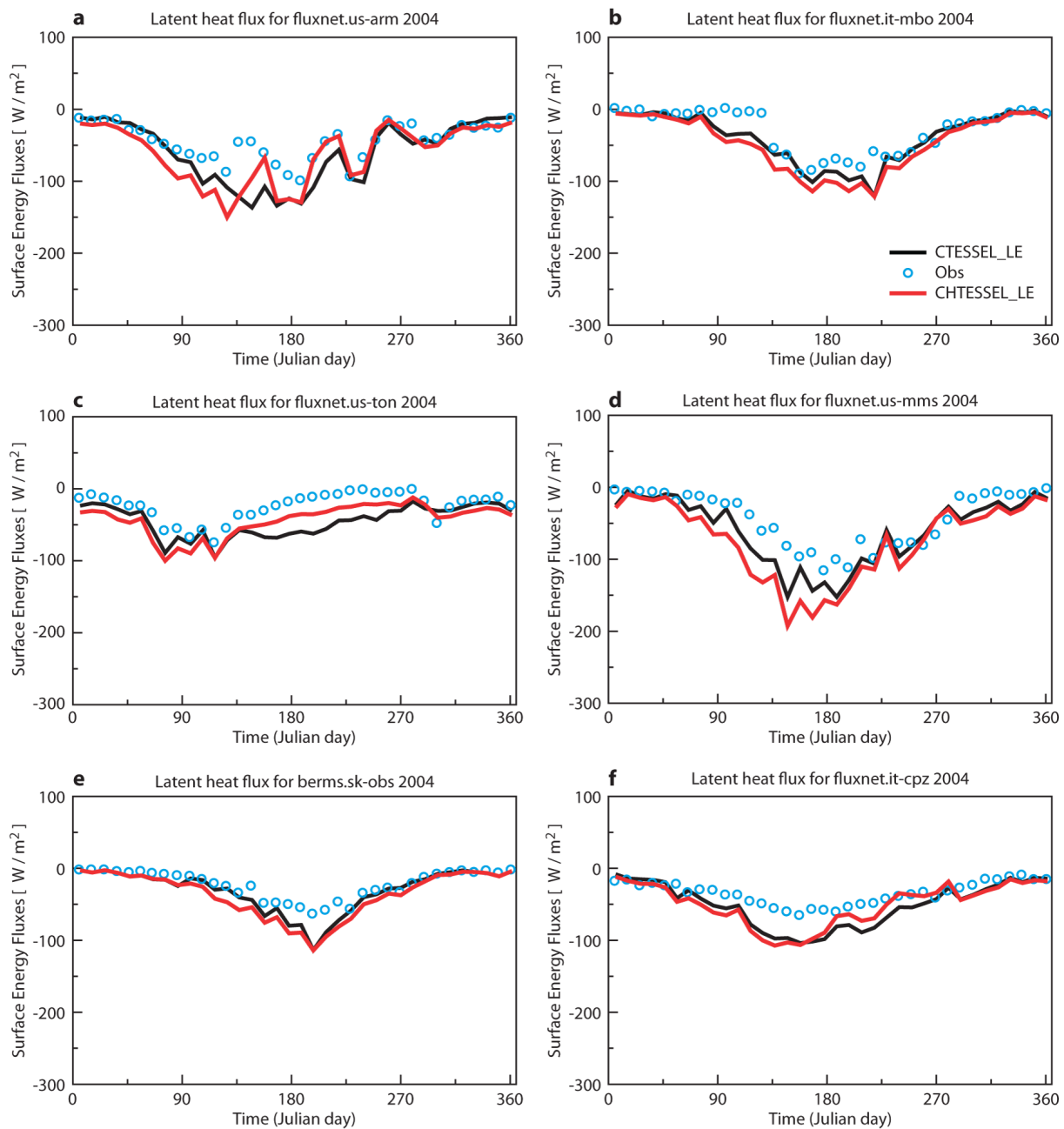


Figure 4: Seasonal cycle (2004) of simulated (lines) and observed (blue dots) latent heat flux [W/m²] for CTESEL (with Ags, black line) and CHTESSEL (with Jarvis-type evaporation, red line) at different observation sites with different biomes: crops (us-arm), grassland (it-mbo), woody savannas (us-ton), deciduous broadleaf forest (us-mms), evergreen needleleaf forest (berms-obs), evergreen broadleaf forest (it-cpz)

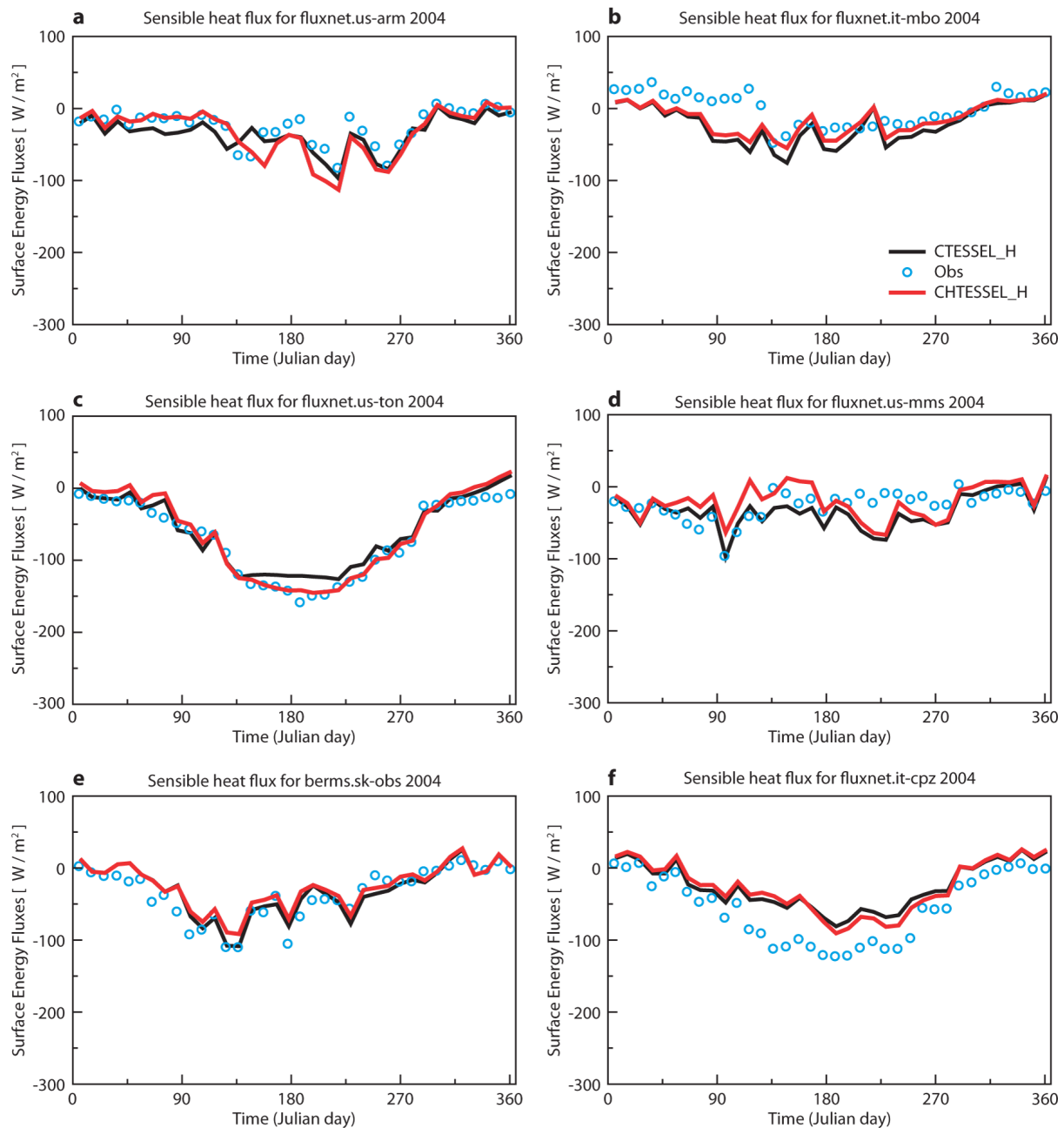


Figure 5: As Figure 4 for the sensible heat flux.

Model	LH rmse	LH bias	LH corr	SH rmse	SH bias	SH corr	NR rmse	NR bias	NR corr
CHTESSEL	28.4	19.5	0.8	23.6	-9.0	0.8	27.2	3.7	0.9
CTESSEL	22.7	13.4	0.8	23.2	-2.9	0.8	27.1	3.9	0.9

Table 4: Average scores for the simulated energy fluxes of CTESSEL and CHTESSEL over the 34 sites.

Figures 6 and 7 show the average diurnal cycle of the latent and sensible heat fluxes in July for the same selected sites. These results confirm that CTESSEL and CHTESSEL have reasonable skills over the considered vegetation types and regions. The correlation between observed and modelled mean diurnal cycle exceeds 0.8 for both the latent and sensible heat flux.

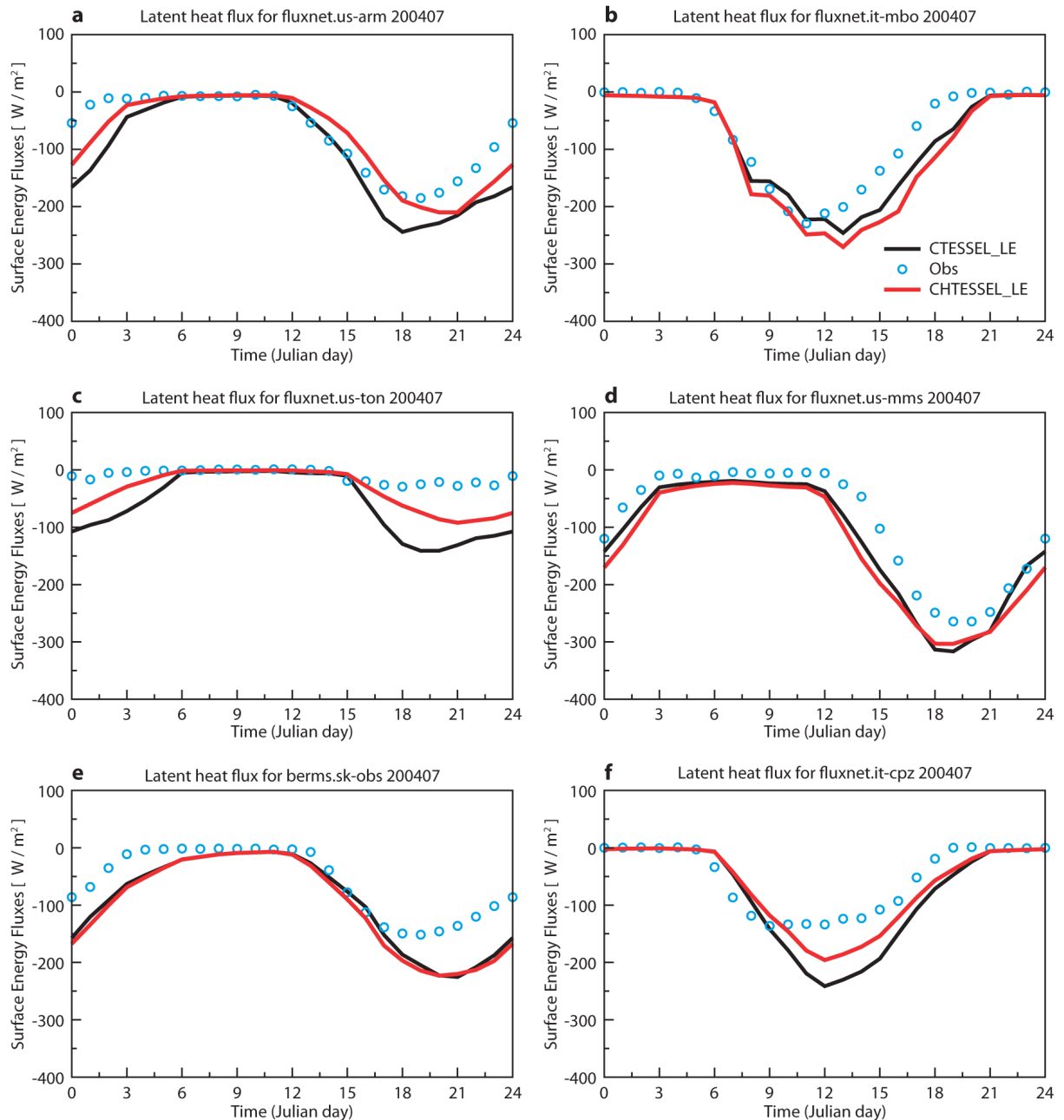


Figure 6: July 2004 average diurnal cycle of Simulated (line) and Observed (blue dots) Latent heat flux [W/m^2] for CTESSEL (with Ags, black line) and CHTESSEL (with Jarvis-type evaporation, red line) at the same observation sites as shown in Figs 4 and 5.

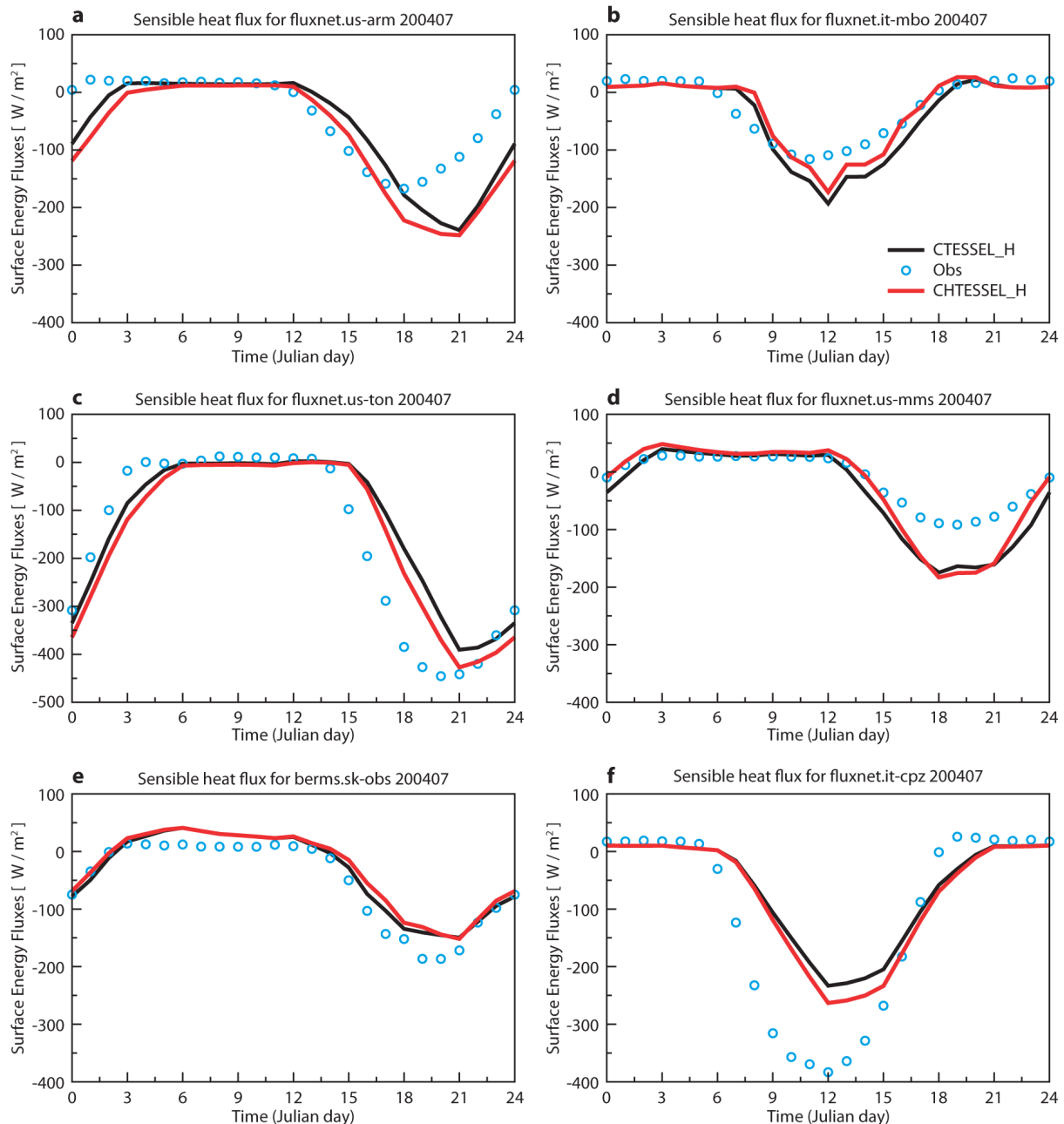


Figure 7: As Figure 6 for the sensible heat flux.

Table 6 shows the statistics of the number of sites where a given model outperforms the other model version. Even though the average scores of CTESEL and CHTESSEL are quite similar, CTESEL has an overall better performance than CHTESSEL for most sites.

Model	GPP rmse	GPP bias	GPP corr	NEE rmse	NEE bias	NEE corr	Reco rmse	Reco bias	Reco corr
CHTESSEL	2.2	0.6	0.8	1.6	-0.1	0.6	1.8	-0.7	0.7
CTESSEL	2.0	0.3	0.8	1.6	-0.3	0.7	1.8	-0.6	0.7
CASA-GFED3	-	-	-	1.8	0.7	0.4	-	-	-

Table 5: - Average scores for the simulated carbon fluxes of CTESSEL, CHTESSEL and over the 34 sites.

Score	Scheme	Number of sites with better performance		
		Latent Heat flux	Sensible Heat flux	Net Ecosystem Exchange
rmse	CTESSEL/CHTESSEL	30/4	19/15	17/17
	CTESSEL/CASA-GFED3	-	-	26/8
	CHTESSEL/CASA-GFED3	-	-	25/9
correlation	CTESSEL/CHTESSEL	17/17	22/12	27/7
	CTESSEL/CASA-GFED3	-	-	26/8
	CHTESSEL/CASA-GFED3	-	-	26/8

Table 6: - Number of sites with better performance corresponding to the 10-day average results of the 3 schemes CTESSEL, CHTESSEL and CASA-GFED3 among the 34 sites.

5.1.2 Natural carbon dioxide fluxes

5.1.2.1 Gross Primary Production and Ecosystem Respiration

As for the energy fluxes, the GPP and Reco fluxes calculated by CTESSEL and CHTESSEL are evaluated with in-situ observed quantities. Although both model versions carry the same carbon flux parameterization, different treatment in transpiration may lead to different CO₂ fluxes. Both GPP and Reco show a generally good performance for 10-day mean values with an average correlation of 0.8 for GPP and 0.7 for Reco (see Figure 8 and Table 5). For some stations both models have rather poor scores. The correspondence between the scores of the two models indicates that the problem is not due to the canopy conductance calculation, but rather to other error sources such as an inadequate representation of the effective coefficients dependent on vegetation type. For instance the Il-Yat site with a mediterranean needleleaf type is represented by parameters for boreal needleleaf forest in the current model set up. The already noted error in the radiative forcing over the tropical region (Fig 3-c) is another likely source of error. For the 6 selected sites, the 2004 seasonal cycles of GPP and Reco are illustrated in Figures 9 and 10 respectively. The figures show that the observed seasonal cycles are reasonably well simulated by both model versions.

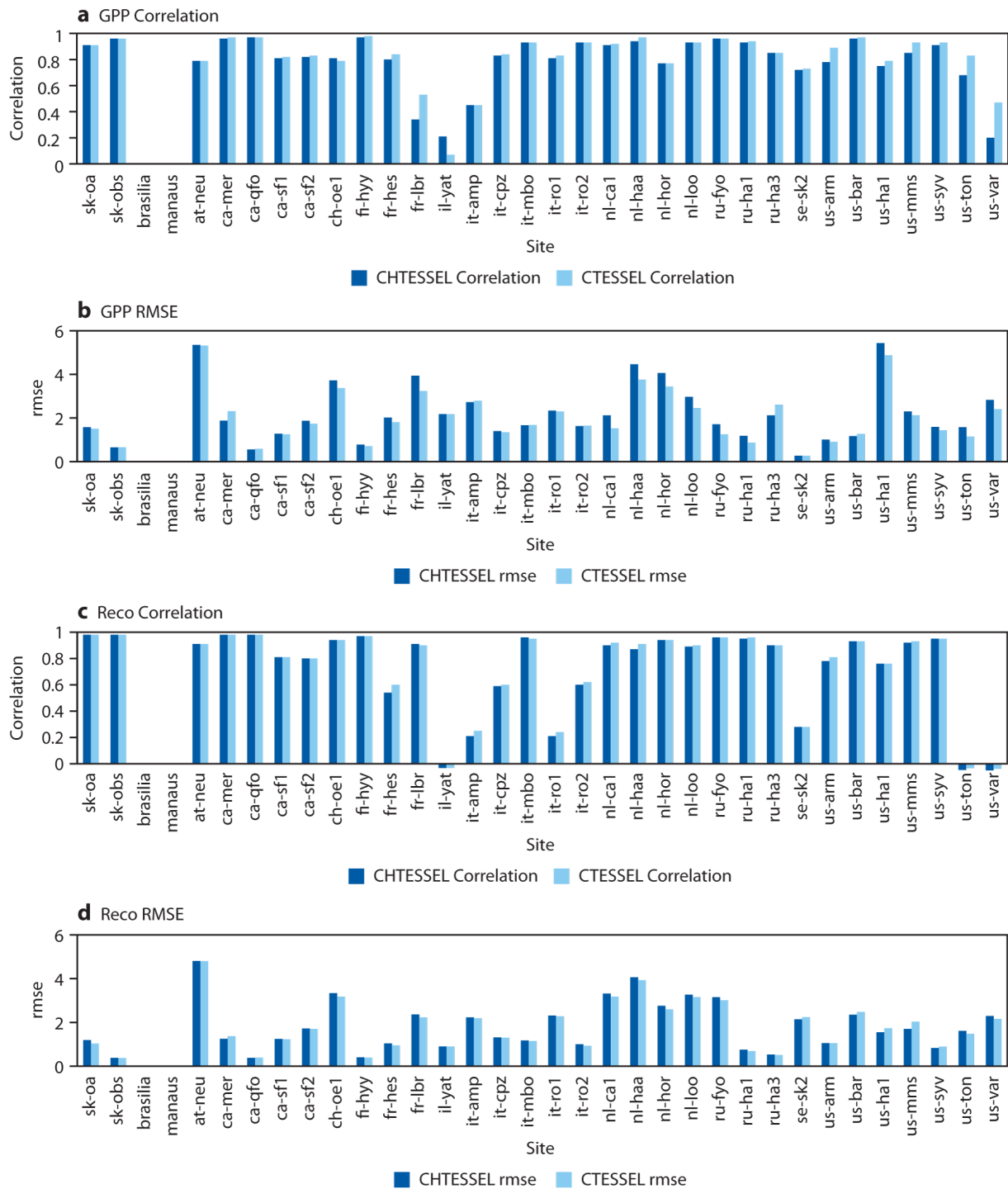


Figure 8: Scores of the simulated carbon fluxes compared with eddy-covariance observation over the 34 sites. Dark blue bars are for CHTESSEL runs, light blue bars are for the CTESSEL results. (a) Gross primary production correlation, (b) Gross primary production rmse, (c) Ecosystem respiration correlation, (d) Ecosystem respiration rmse

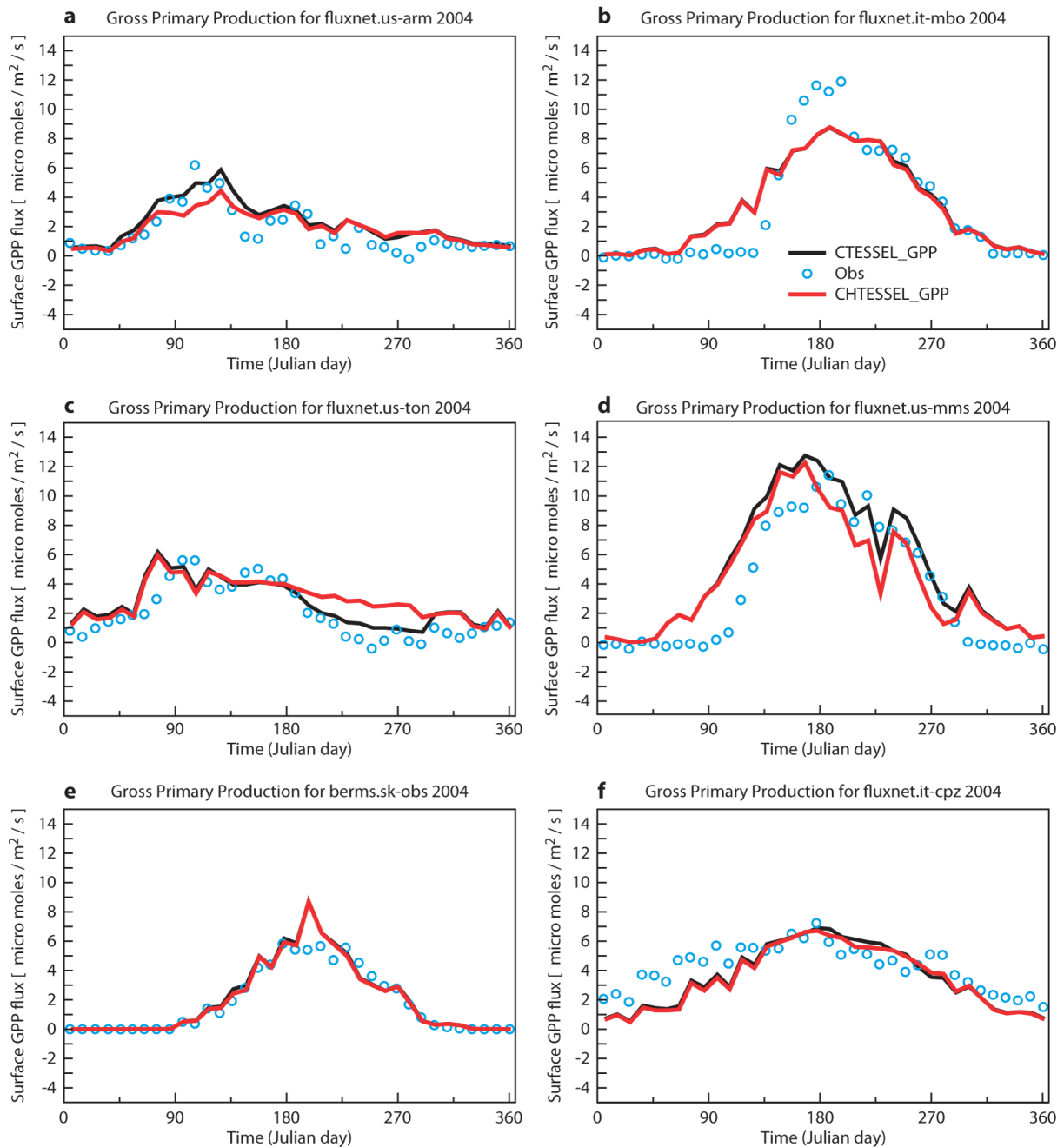
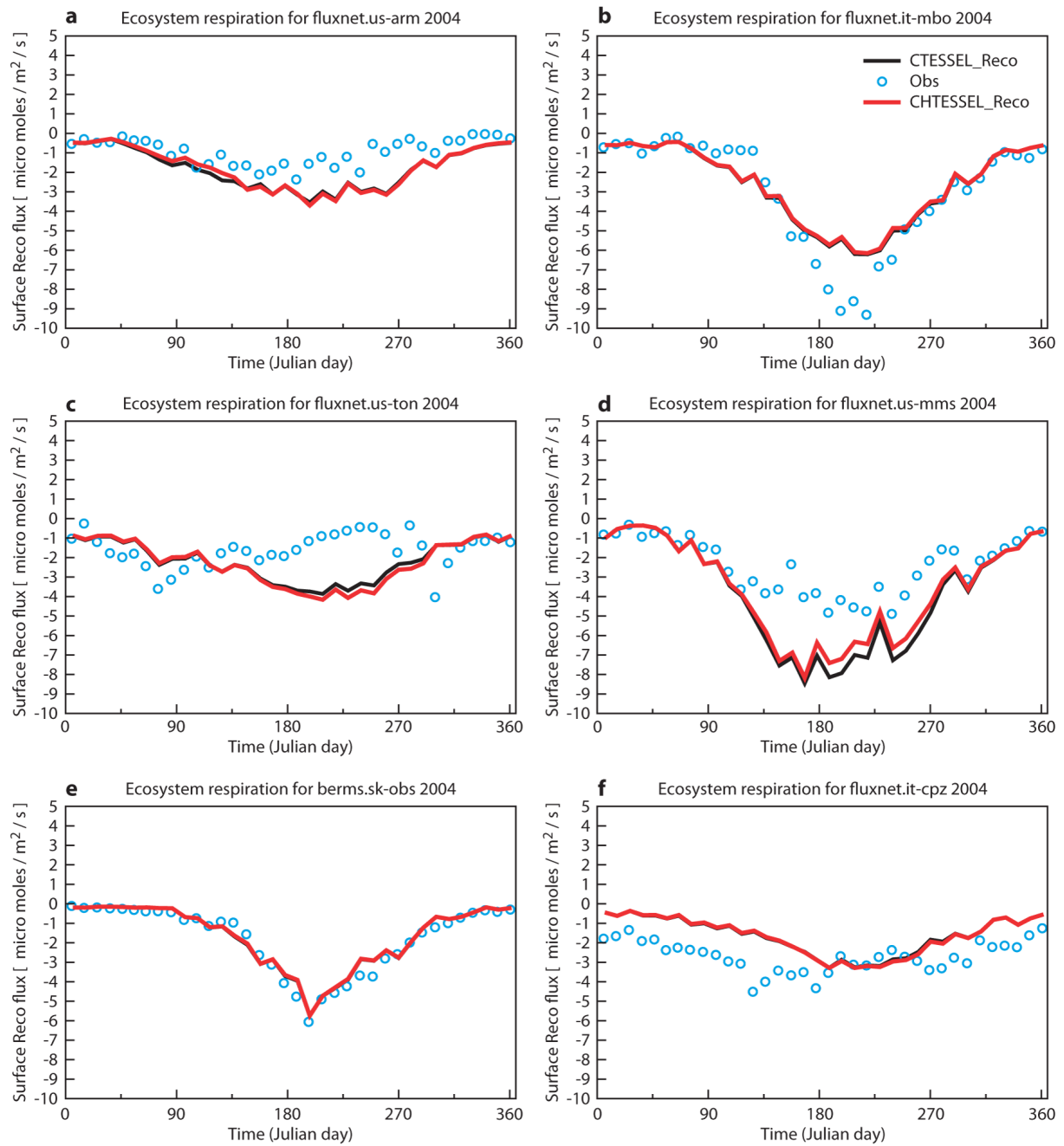


Figure 9: Seasonal cycle (2004) of 10-day averaged simulated (lines) and observed (blue dots) gross primary production GPP [$\mu\text{mol m}^{-2} \text{s}^{-1}$], for CTESSEL (with Ags, black line) and CHTESSEL (with Jarvis-type evaporation, red line) at different observation sites with different biomes as indicated in Fig 4.

Figure 10: As Figure 9 for the ecosystem respiration R_{eco} [$\mu\text{moles m}^{-2} \text{s}^{-1}$].

5.1.2.2 Net Ecosystem Exchange

The Net Ecosystem Exchange (NEE) is a useful quantity for the computation of atmospheric CO₂ concentration, since it represents important land sources and sinks of CO₂. CTESSEL and CHTESSEL results are compared with the Global Fire Emissions Database (GFED3.0)-Carnegie-Ames-Stanford-Approach (CASA) NEE outputs (CASA-GFED3; see Van der Werf et al. 2010 and Potter et al. 1993). Prior to the calculating the comparison statistics, CASA-GFED3 data are disaggregated to a 3-hourly timestep.

Similar to the energy fluxes, both model versions are comparable over the 34 sites in 2004 (Table 5) with slightly better scores for CTESSEL (Table 6). The comparison with in situ observations yields similar results for CHTESSEL and CTESSEL with an average rmse of 1.6 $\mu\text{mol m}^{-2} \text{s}^{-1}$, which is slightly better than the rmse of 1.8 $\mu\text{mol m}^{-2} \text{s}^{-1}$ for the CASA-GFED3 results (Figure 11).

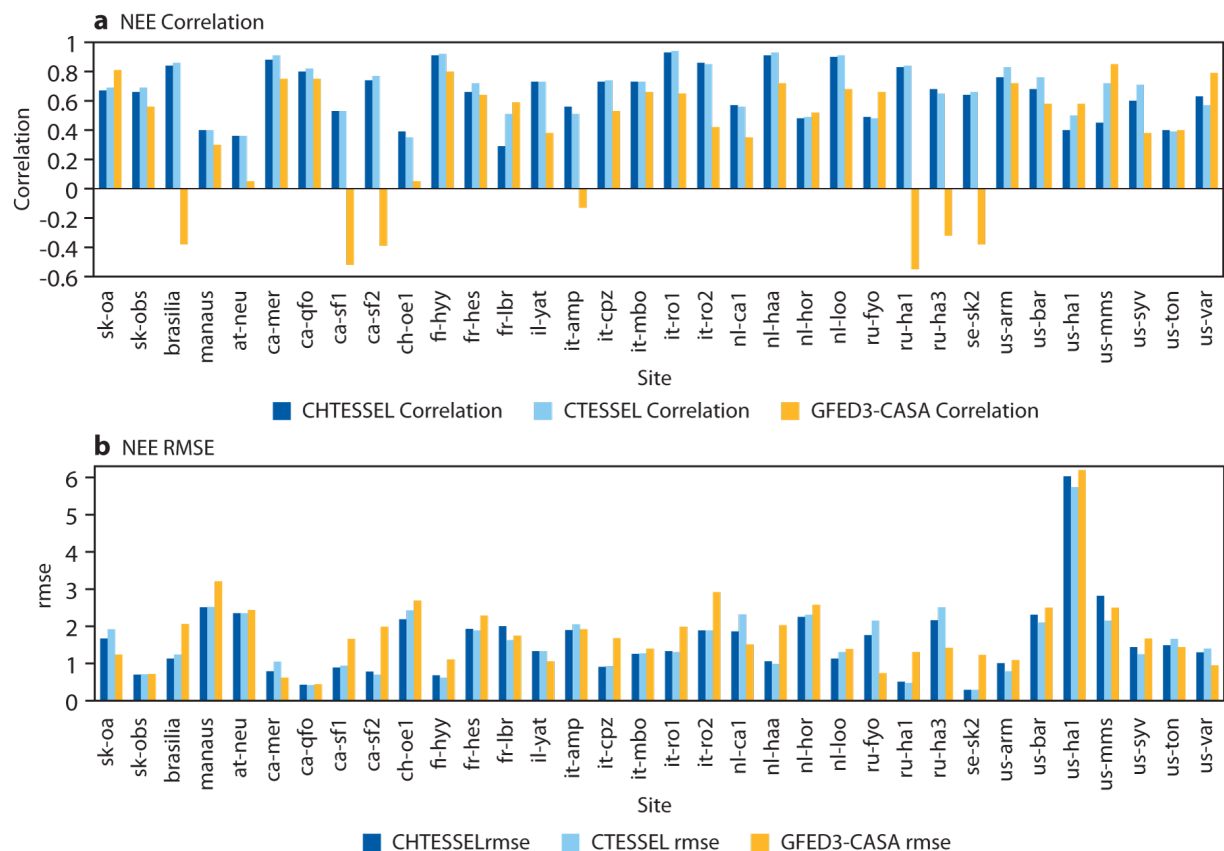


Figure 11: Scores of the simulated carbon net ecosystem exchange with eddy-covariance observations over the 34 sites. Dark blue bars are for CHTESSEL runs, light blue bars are for the CTESSEL results and yellow bars are for the CASA-GFED3 data. (a) correlation, (b) rmse [$\mu\text{mol m}^{-2} \text{s}^{-1}$].

The NEE seasonal cycle for 2004 at the 6 selected sites is shown in Figure 12. The average diurnal cycle for the month of July is shown in Figure 13. These results obtained with the Jarvis based evaporation in CHTESSEL indicates that the simulation of the photosynthesis process although tightly

linked to the transpiration, could be performed in a modular way and lead to comparable results as from the photosynthesis based evaporation in CTESSEL.

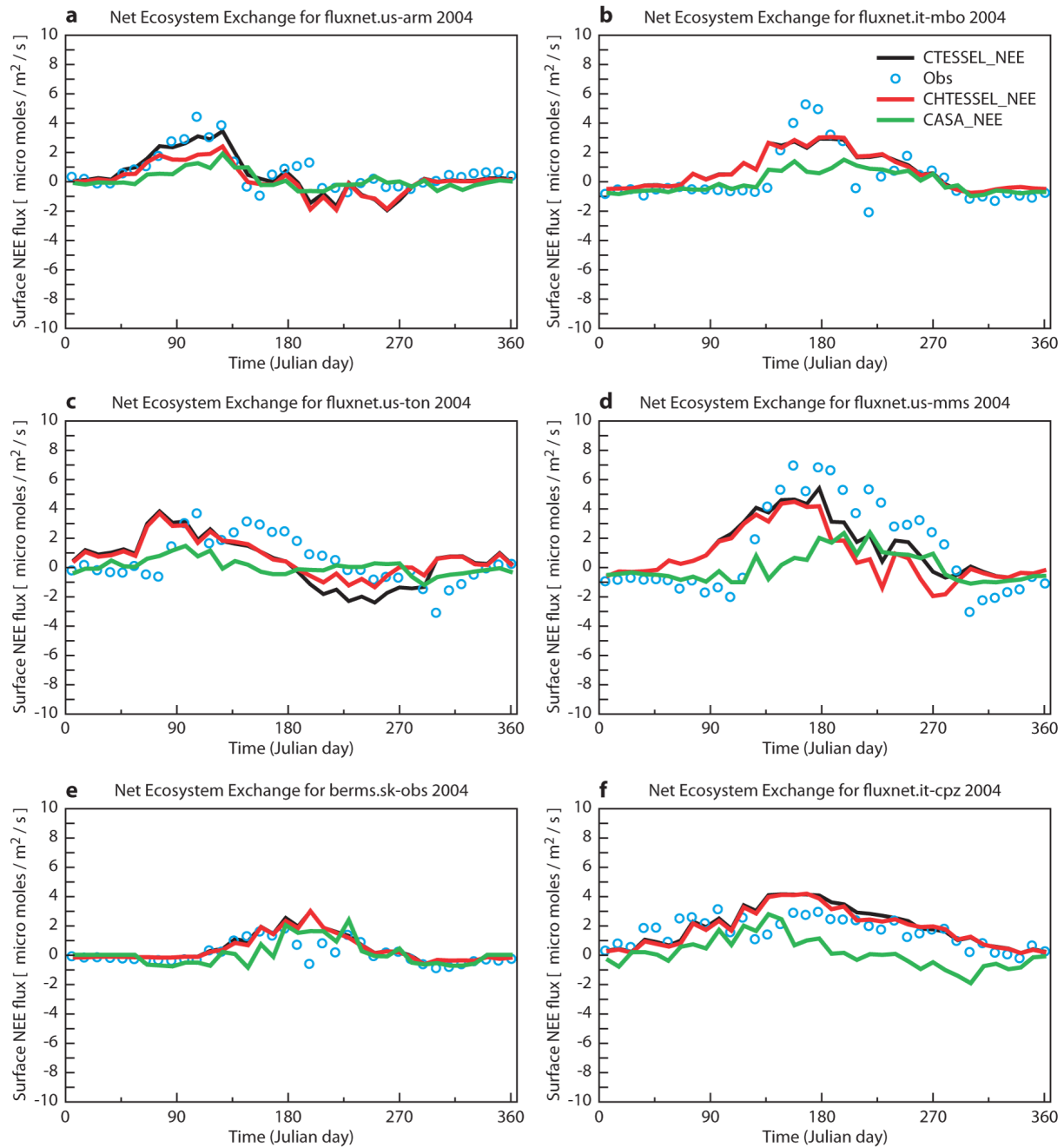


Figure 12: As Figure 9 for the net ecosystem exchange NEE [$\mu\text{mol m}^{-2} \text{s}^{-1}$].

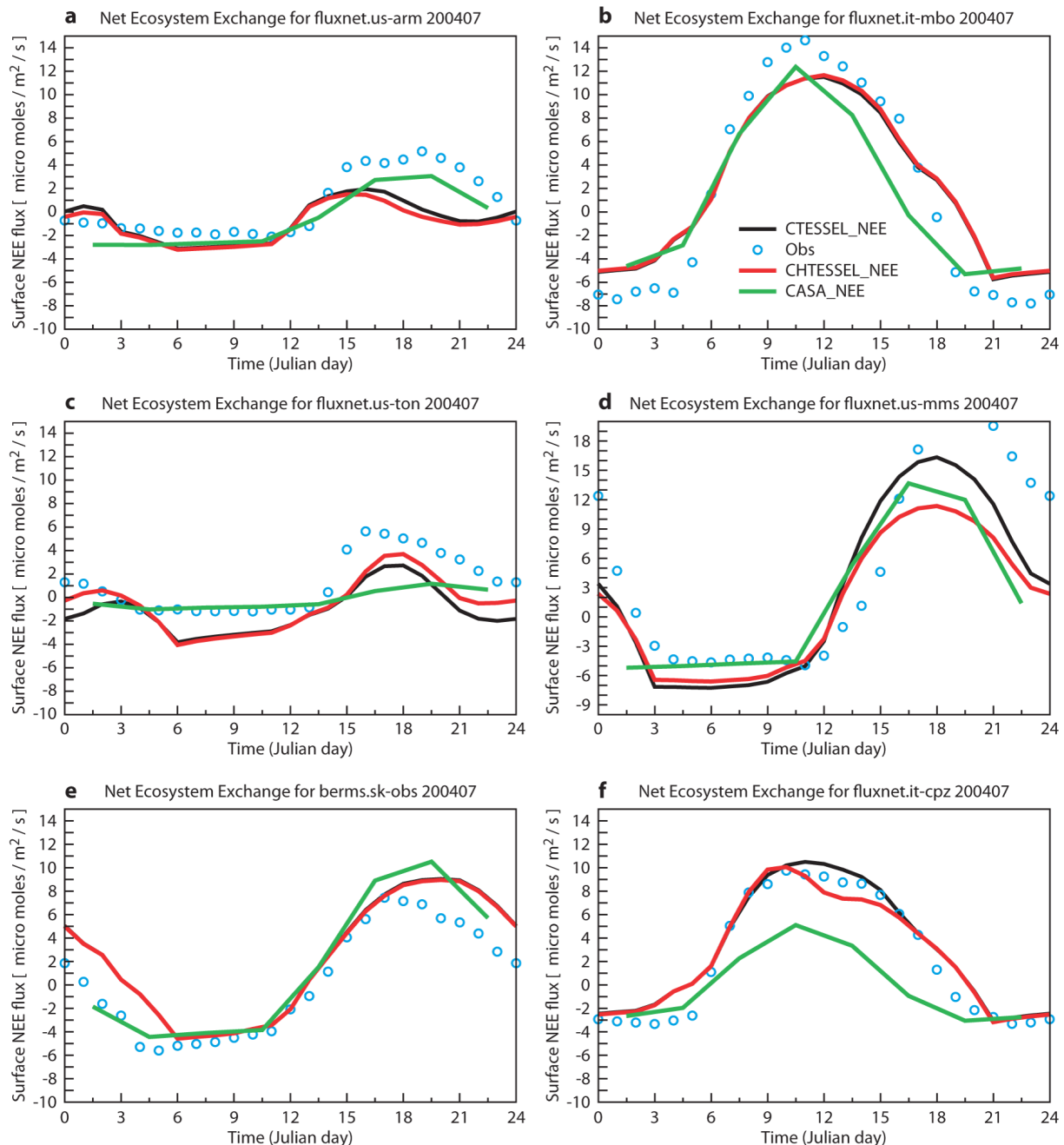


Figure 13: Simulated and observed mean July diurnal cycle of the net ecosystem exchange NEE [$\mu\text{mol m}^{-2} \text{s}^{-1}$].

5.2 Multi-annual global offline simulations

As shown in the previous section, the selection between the two model versions has a near-neutral impact on the evapotranspiration while the skill in predicting NEE is similar. For this reason, CHTESSEL, which would preserve the actual weather prediction skills, was introduced in the operational IFS, and results of this configuration are shown hereafter. Figure 14 shows global patterns of January and June NEE averages over the 2003-2008 period as simulated by CHTESSEL and CASA-GFED3. In January, although the two models predict an emission of carbon from the Northern Hemisphere, NEE is less pronounced in CHTESSEL partly owing to the snow attenuation function introduced in the ecosystem respiration formulation (section 3). In the tropics, the two models disagree: CHTESSEL simulates an uptake of CO₂ whereas CASA-GFED3 predicts a release particularly in the Amazonian region. In June, CASA-GFED3 and CHTESSEL predict an uptake of CO₂ over the Northern Hemisphere with similar spatial patterns, although CHTESSEL shows more spatial variability. Over the Amazonian tropics, the models disagree in June. Apart from differences in the model formulations, these differences may be associated to the meteorological forcing, in particular over the tropics. Zhao et al. (2006) showed that using the MODIS GPP algorithm, the annual Net Primary Production over the Amazonian region can vary by more than 50% depending on the forcing used.

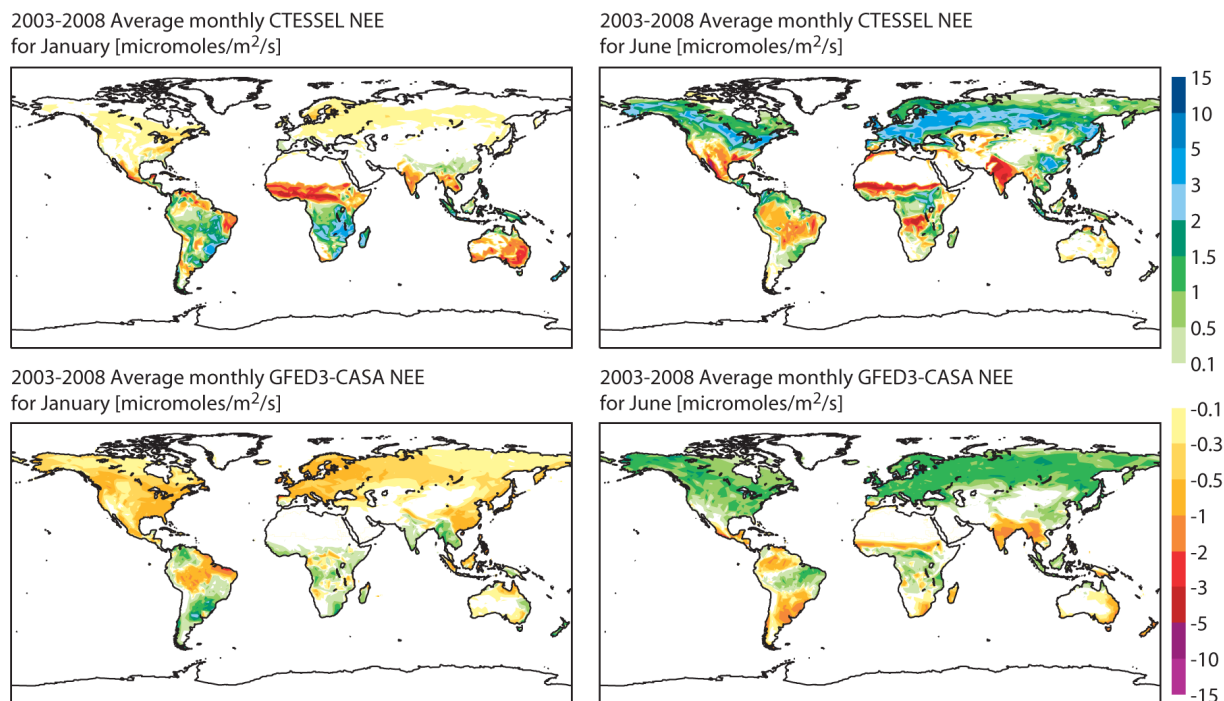


Figure 14: 2003-2008 monthly average of the Net Ecosystem Exchange [$\mu\text{mol m}^{-2} \text{s}^{-1}$] simulated by CHTESSEL (upper panels) and CASA-GFED3 (lower panels) for January (left panels) and June (right panels).

To assess the global CO₂ budget from the surface as simulated by CHTESSEL, Figure 15 shows a comparison with budgets from known land surface models and several state-of-the-art flux inversion systems for the period 2002 - 2004. Despite the large differences in the formulation of the various models and flux inversion systems, the CHTESSEL budget is within the range of the listed estimations and reveals an inter-annual variability consistent with the other inventories. The simple parameterization of the respiration (meant to avoid long spin-up windows not suitable in NWP) and the absence of land use change (which is a reasonable assumption for the considered period 2002-2004) in CHTESSEL in combination with an accurate atmospheric forcing lead to realistic simulations of the yearly terrestrial carbon sink and its interannual variability.

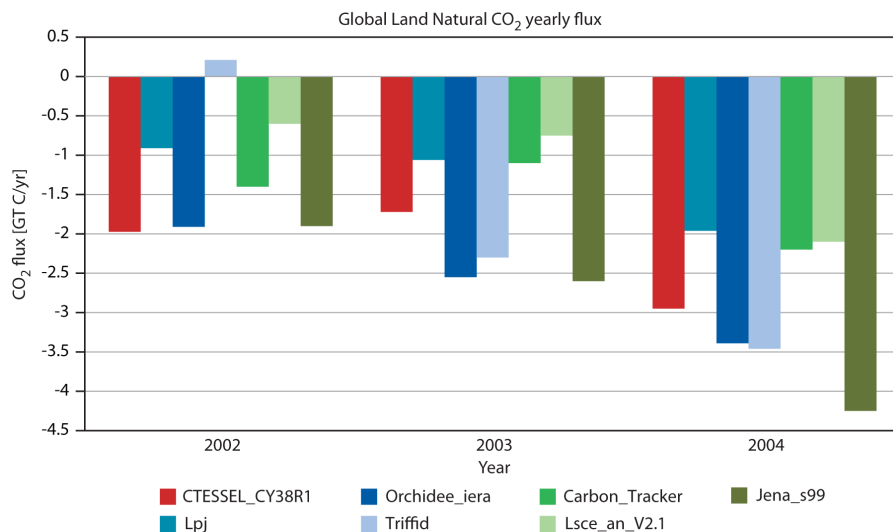


Figure 15: Global land annual mean natural CO₂ flux [Gt-C/yr] estimated from inverse modelling (carbon tracker: dark green, LSCE version 2.1: light green, Jena s99: evergreen) and land surface models (Trifid: light blue, LPJ: intermediate blue, ORCHIDEE: dark blue) compared to CTESSEL (red colour). Values used in this figure are obtained from the CarboScope website: http://www.carboscope.eu/?q=flux_ts¶m=co2_dgvm (Sitch et al. 2008).

5.3 Impact of CO₂ fluxes on Atmospheric concentrations

Terrestrial NEE fluxes are used as a lower boundary condition for atmospheric CO₂ concentrations with the atmospheric general circulation model used in the MACC project. The terrestrial biospheric CO₂ exchange is one of the most important components modulating the interannual variability of atmospheric CO₂ growth (Knorr et al., 2007, Le Quéré et al., 2009). In this evaluation the impact of NEE on atmospheric CO₂ is integrated in space and time and allows evaluation of the resulting concentrations with independent atmospheric CO₂ concentration observations.

The impact of terrestrial NEE from CHTESSEL is compared to results obtained using NEE from CASA GFED3 (Engelen et al., 2009). A tracer transport model with prescribed surface fluxes for the ocean (Takahashi et al., 2009), biomass burning (GFED3.0, van der Werf et al., 2010), and anthropogenic emissions (EDGARv4.2, Olivier and Berdowski 2001) is used for this. The tracer transport model is based on IFS (currently operational at ECMWF) with 60 model levels and a horizontal resolution of approximately 78 km.

The global land annual NEE budget from CHTESSEL and CASA-GFED3 are compared in Figure 16 together with the atmospheric growth obtained from observations (GLOBALVIEW-CO₂, 2010). The CHTESSEL NEE is of similar magnitude as CASA-GFED3. However, both the interannual variability of CHTESSEL NEE and the resulting total CO₂ flux -obtained by combining the NEE with the other prescribed CO₂ surface fluxes in the model (not shown)- have a consistently better correlation with the interannual variability of the atmospheric growth based on observations (0.7 for the total flux based on CHTESSEL NEE and 0.2 for the total flux based on CASA-GFED3 NEE). The atmospheric CO₂ latitudinal distribution and seasonal cycle from the simulation using CHTESSEL NEE is also consistent with that from CASA-GFED3 (Figure 17). Both CHTESSEL and CASA-GFED3 underestimate the CO₂ sink in the Northern Hemisphere (NH) summer, but CHTESSEL shows a better match to GLOBALVIEW-CO₂ in the NH winter.

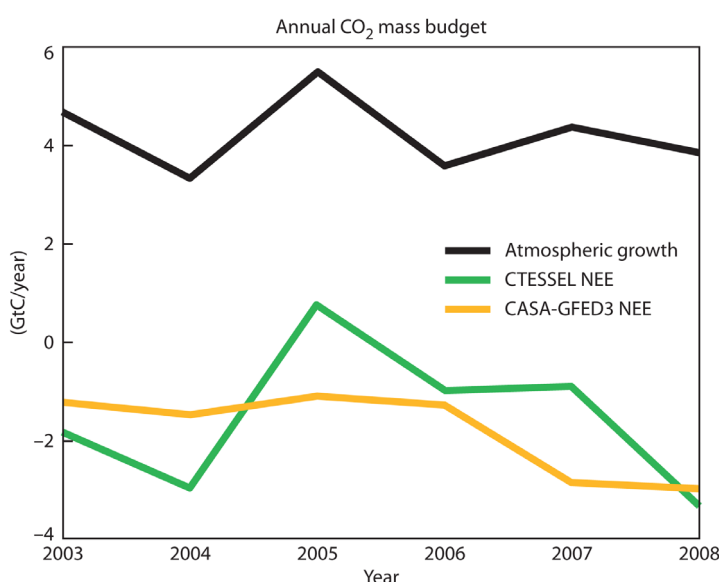


Figure 16: Annual global NEE from CHTESSEL (green), NEE from CASA-GFED3 (yellow), and the observed CO₂ atmospheric growth (black) [GLOBALVIEW-CO₂, 2010] for the period from 2003 to 2008.

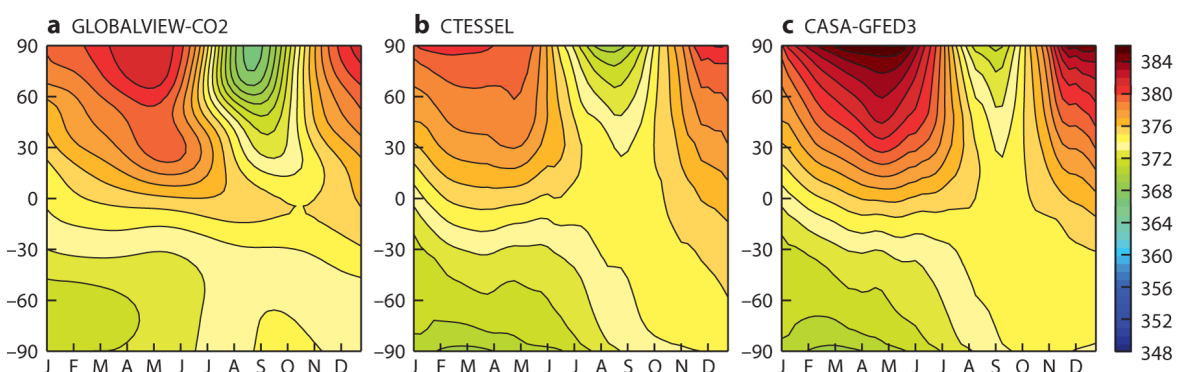


Figure 17: Hovmöller diagram of weekly atmospheric CO₂ concentrations [ppm] for the year 2003 across latitude from (a) the NOAA GLOBALVIEW-CO₂ product based on observations and the model forecasts using (b) CHTESSEL NEE and (c) CASA-GFED3 NEE.

6 Discussion and Conclusions

This study describes the stomatal conductance and carbon dioxide exchange module added to the ECMWF LSM HTESSEL. The modules enable to simulate the surface energy exchange in terms of sensible and latent heat flux along with the biospheric gross primary production (GPP) and the ecosystem respiration (Reco). The latter two quantities are components of the biospheric Net Ecosystem Exchange (NEE) that can provide the surface boundary condition to atmospheric CO₂ transport models.

The scheme is calibrated by optimizing the parameters that actively control the CO₂ fluxes using observations of surface energy and CO₂ fluxes for a range of vegetation types. The model is then validated using results from a different time period on the same sites. Two versions of the new scheme are considered in the study: one uses a photosynthesis based parameterisation where evaporation and photosynthesis interact (CTESSEL), and in the other the evaporation processes are treated independently from photosynthesis with a Jarvis based canopy conductance formulation (CHTESSEL).

The comparison of the simulated fluxes at the field-sites with the CASA-GFED3 products shows that the land model generally outperforms this inventory. This result is consistent with Balzarolo et al. (2011) who found that being optimized by vegetation types, CTESSEL and CHTESSEL also outperform two other models (ISBA-Ags and ORCHIDEE) over a multiannual period at the field-site scale. The comparison between CTESSEL and CHTESSEL showed that the separation of the evapotranspiration and CO₂ exchange processes does not significantly affect the overall results and therefore enables to model terrestrial CO₂ exchange in NWP models without impact on other land surface processes that might affect weather prediction. The full coupling of CO₂ and evapotranspiration is therefore not a pre-condition to model NEE with reasonable success. However, given the slight improvement seen with a fully photosynthesis based parameterisation, its coupling within operational NWP such as the IFS is a straightforward step. Further analysis could be performed to assess whether the inclusion of more interaction between the environmental factors is the main cause of more realistic variability of the turbulent fluxes at both seasonal and diurnal time scales. At present, a temperature response is not included in the actual Jarvis-based formulation. We note that the photosynthesis approach by definition includes a physiological response of stomatal conductance to atmospheric CO₂, which is known to be increasing at present. This model feature could be an advantage of the A-gs approach over the Jarvis-based approach.

The global evaluation shows that CHTESSEL can predict the spatial and seasonal variability of NEE reasonably well. Its global budget is within the range of uncertainty of other products from state-of-the-art land vegetation models and flux inversion systems. Furthermore, its coupling with an atmospheric CO₂ transport model shows that its variability correlates well with observed CO₂ atmospheric variability at global and seasonal to interannual scales. These results indicate that even though the respiration is parameterized in a simple way and does not account for land use change (which is a reasonable assumption for short time scales), the CHTESSEL model in combination with an accurate atmospheric forcing is able to simulate the yearly terrestrial carbon sink and its interannual variability reasonably well. The rather good performance of the CTESSEL/CHTESSEL model compared to flux towers and in terms of inter-annual variability, suggests that the model captures the basic dependencies on environmental parameters very well. Furthermore it is believed that the

coupling to the NWP meteorological forcing brings a benefit because over the years a lot of attention has been paid in NWP research to the analysis of atmospheric and soil variables like temperature, atmospheric moisture, and soil moisture. Also radiation and precipitation fields from NWP type re-analysis are shown to be reliable (Balsamo et al., 2010, Szczypta et al., 2011).

The leaf area index data used in this study is based on a climatology extracted from satellite observations. Inclusion of an interaction between net vegetation carbon gain and LAI could be helpful in further constraining NEE estimates by data assimilation of LAI derived from satellite observations. The prior spatial distribution of surface fluxes is essential to obtain an improved accuracy of inverse modelling results (Chevallier et al., 2012). A two-way interaction between the forward land surface modelling and atmospheric model inversion is seen as one of the important CO₂ modelling perspectives. With its simple parameterization and operational implementation CTESSEL/CHTESSEL is believed to be well suited to such objective.

Acknowledgements

This work used eddy covariance data acquired by the FLUXNET community and that entered the LaThuile Open-Access synthesis dataset available via the web-site (<http://www.fluxdata.org>). We gratefully acknowledge all the PIs (see Table 3) at all the sites from which data were taken for this study and the institutions and agencies that support data collection at these sites.

We would also thank The Fluxnet-Canada Research Network for making available the BERMS data (<http://berms.ccrp.ec.gc.ca/Overview/e-overview-about.htm>), as well as the PIs and researcher involved in the CEOP project for provision and archiving the data used in this study (<http://www.ceop.net/>).

This work is a contribution to the GEOLAND-2 project, funded by the European Commission 7th Framework Programme in preparation to the Global Monitoring for Environment and Security (GMES) initiative.

References

- Albergel, C., J.-C. Calvet, A.-L. Gibelin, S. Lafont, J.-L. Roujean, C. Berne, O. Traulle, and N. Fritz, (2010), Observed and modelled ecosystem respiration and gross primary production of a grassland in south-western France. *Biogeosciences*, **7**, 1657–1668.
- Ammann, C., C. Flechard, J. Leifeld, A. Neftel, J. Fuhrer, (2007), The carbon budget of newly established temperate grassland depends on management intensity. *Agric. Ecos. Environ.*, **121**, 5-20.
- Baker, I. T., A. S. Denning, N. Hanan, L. Prihodko, P.-L. Vidale, K. Davis, and P. Bakwin, (2003), Simulated and observed fluxes of sensible and latent heat and CO₂ at the WLEF-TV Tower using SiB2.5. *Glob. Change Biol.*, **9**, 1262–1277.

- Baldocchi, D., et al., (2001), FLUXNET: A new tool to study the temporal and spatial variability of ecosystem-scale carbon dioxide, water vapor, and energy flux densities, *Bull. Am. Meteorol. Soc.*, **82**, 2415-2434, doi:10.1175/1520-0477.
- Baldocchi D., (2008), Breathing of the terrestrial biosphere: lessons learned from a global network of carbon dioxide flux measurement systems. *Aust. J. Bot.*, **56**, 1–26.
- Ball, J. T., I. E. Woodrow, and J. A. Berry, (1987), A model predicting stomatal conductance and its contribution to the control of photosynthesis under different environmental conditions, in: *Progress in photosynthesis research*, edited by: Biggins, I., Martinus Nijhoff, Netherlands, 221–224.
- Balsamo, G., S. Boussetta, P. Lopez, L. Ferranti, (2010), Evaluation of ERA-Interim and ERA-Interim GPCP-rescaled precipitation over the U.S.A., *ERA Report Series*, **5**, pp10.
- Balsamo, G., P. Viterbo, A. Beljaars, B. van den Hurk, M. Hirschi, A.K. Betts, and K. Scipal, (2009), A Revised Hydrology for the ECMWF Model: Verification from Field Site to Terrestrial Water Storage and Impact in the Integrated Forecast System. *J. Hydrometeorol.*, **10**, 623-643.
- Balsamo, G., S. Boussetta, E. Dutra, A. Beljaars, P. Viterbo, B. Van den Hurk, (2011): Evolution of land surface processes in the IFS, *ECMWF Newsletter*, **127**, 17-22.
- Balzarolo, M., G. Balsamo, A. Barbu, S. Boussetta, J.-C. Calvet, A. Cescatti, F. Chevallier, S. Lafont, F. Maignan, J. De Vries, L. Kullman, D. Papale, (2011), In-situ verification and comparison of three models for predicting carbon and water fluxes across ecosystems. *Proceeding of the 3rd iLEAPS Science Conference* Garmisch-Partenkirchen, Germany 18-23 September 2011.
- Beljaars, A.C.M., and P. Viterbo, (1999), Soil moisture-precipitation interaction: Experience with two land surface schemes in the ECMWF model. In: *Global energy and water cycles* edited by K. Browning and R. Gurney, Cambridge University Press, Cambridge, 223-233.
- Berbigier P., J.M. Bonnefond, P. Mellmann, (2001), CO₂ and water vapour fluxes for 2 years above Euroflux forest site. *Agric. For. Meteorol.*, **108** (3), 183-197.
- Bergeron, O., H.A. Margolis, T.A. Black, C. Coursolle, A.L. Dunn, A.G. Barr, S.C. Wofsy, (2007), Comparison of CO₂ fluxes over three boreal black spruce forests in Canada. *Global Change Biology*, **13**, 89-107, doi:10.1111/j.1365-2486.2006.01281.x.
- Berry, J.A. and J.K. Raison, (1982), Responses of Macrophytes to Temperature. *Encyclopedia of plant Physiology, New Series, Physiological plant Ecology II*, **12B**, 277-388.
- Betts, A.K., J.H. Ball, A.C.M. Beljaars, M.J. Miller, and P.A. Viterbo, (1996), The land-surface-atmosphere interaction: A review based on observational and global modelling perspective. *J. Geophys. Res.*, **101**, 7209-7225.

- Betts, A.K., J.H. Ball, A.G. Barr, T.A. Black, J.H. McCaughey and P. Viterbo, (2006): Assessing land-surface-atmosphere coupling in the ERA-40 re-analysis with boreal forest data, *Agric. For. Meteorol.*, **140**, 355–382.
- Blyth, E. M, J. H. C. Gash, A. Lloyd, M. Pryor, G. P. Weedon, and J. W. Shuttleworth, (2010), Evaluating the JULES model energy fluxes using FLUXNET data, *J. Hydrometeorol.*, **11**, 509–519.
- Bonan, G. B., and S. Levis, (2010), Quantifying carbon-nitrogen feedbacks in the Community Land Model (CLM4), *Geophys. Res. Lett.*, **37**, L07401, doi:10.1029/2010GL042430.
- Boussetta, S., T. Koike, Y. Kun, T. Graf and M. Pathmathevan, (2008), Developement of a coupled land-atmosphere satellite data assimilation system for improved local atmospheric simulations. *Rem. Sens. Envir.*, **112**, 720–734.
- Boussetta, S., G. Balsamo, A. Beljaars, T. Kral and L. Jarlan, (2011), Impact of a satellite-derived Leaf Area Index monthly climatology in a global Numerical Weather Prediction model, *Int. J. Rem. Sens.* (accepted), also available as *ECMWF Tech. Memo.* **640**.
- Calvet J.C., J. Noilhan, J.-L. Roujean, P. Bessemoulin, M. Cabelguenne, A. Olioso, J.-P. Wigneron, (1998), An interactive vegetation SVAT model tested against data from six contrasting sites. *Agric. For. Meteorol.*, **92**, 73–95.
- Calvet, J.-C., (2000), Investigating soil and atmospheric plant water stress using physiological and micrometeorological data, *Agric. For. Meteorol.*, **103**, 229–247.
- Calvet, J.-C., V. Rivalland, C. Picon-Cochard and J.M. Guehl, (2004), Modelling forest transpiration and CO₂ fluxes – response to soil moisture stress. *Agric. For. Meteorol.*, **124**, 143–156.
- Chevallier, F., T. Wang, P. Ciais, F. Maignan, M. Bocquet, M. A. Arain, A. Cescatti, J. Chen, A. J. Dolman, B. E. Law, H. A. Margolis, L. Montagnani, E. J. Moors, (2012), What eddy-covariance measurements tell us about prior land flux errors in CO₂-flux inversion schemes, *Glob. Biogeochem. Cyc.*, **26**, GB1021, doi:10.1029/2010GB003974.
- Clark, D. B., L. M. Mercado, S. Sitch, C.D. Jones, N. Gedney, M. J. Best, M. Pryor, G. G. Rooney, R. L. H. Essery, E. Blyth, O. Boucher, R. J. Harding, C. Huntingford and P.M. Cox, (2011), The Joint UK Land Environment Simulator (JULES), model description – Part 2: Carbon fluxes and vegetation dynamics, *Geosci. Mod. Dev.*, **4**, 701–722, doi:10.5194/gmd-4-701-2011, 2011
- Collatz, G.J, M. Ribas-Carbo and J.A. Ball, (1992), Coupled photosynthesis-stomatal conductance model for leaves of C4 plants. *Aust. J. Plant Physiol.*, **19**, 519–538.
- Cox, P. M., R. A. Betts, C. D. Jones, S. A. Spall, and I. J. Totterdell, (2000), Acceleration of global warming due to carbon-cycle feedbacks in a coupled climate model, *Nature*, **408**, 184–187.
- Dee, D. P., S. M. Uppala, A. J. Simmons, P. Berrisford, P. Poli, S. Kobayashi, U. Andrae, M. A. Balmaseda, G. Balsamo, P. Bauer, P. Bechtold, A. C. M. Beljaars, L. van de Berg, J. Bidlot, N.

- Bormann, C. Delsol, R. Dragani, M. Fuentes, A. J. Geer, L. Haimberger, S. Healy, H. Hersbach, E. V. Hólm, L. Isaksen, P. Kållberg, M. Köhler, M. Matricardi, A. P. McNally, B. M. Monge-Sanz, J.-J. Morcrette, C. Peubey, P. de Rosnay, C. Tavolato, J.-N. Thépaut, F. Vitart, (2011), The ERA-Interim reanalysis: Configuration and performance of the data assimilation system, *Q. J. R. Meteorol. Soc.*, doi: 10.1002/qj.828, also available as *ERA Report Series*, **9**, pp. 71.
- Dutra, E., G. Balsamo, P. Viterbo, P.M.A. Miranda, A. Beljaars, C. Schär, K. Elder, (2010), An improved snow scheme for the ECMWF land surface model: description and offline validation. *J. Hydrometeor.* **11**, 899-916. doi: 10.1175/2010JHM1249.1.
- Engelen, R. J., S. Serrar, and F. Chevallier, (2009), Four-dimensional data assimilation of atmospheric CO₂ using AIRS observations, *J. Geophys. Res.*, **114**, D03303, doi:10.1029/2008JD010739.
- Farquhar, G. D., and T. D. Sharkey, (1982), Stomatal Conductance and photosynthesis. *Ann. Rev. Plant Physiol.*, **33**, 317-345.
- Fischer, M.L, D. P. Billesbach, W. J. Riley, J. A. Berry, and M.S. Torn, (2007). Spatiotemporal Variations in Growing Season Exchanges of CO₂, H₂O, and Sensible Heat in Agricultural Fields of the Southern Great Plains. *Earth Interactions*, **11**, 1-21
- GEOLAND2, (2009), Integrated GMES project on Land Cover and Vegetation, <http://www.gmes-geoland.info>.
- Gibelin, A., J.-C. Calvet, J.-L. Roujean, L. Jarlan, and S. O. Los, (2006), Ability of the land surface model ISBA-A-gs to simulate leaf area index at the global scale: Comparison with satellites products, *J. Geophys. Res.*, **111**, D18102, doi:10.1029/2005JD006691.
- GLOBALVIEW-CO₂, (2010), Cooperative Atmospheric Data Integration Project – Carbon Dioxide. CD-ROM, NOAA ESRL, Boulder, Colorado [Also available on Internet via anonymous FTP to ftp.cmdl.noaa.gov, Path : ccg/co2/GLOBALVIEW], 2010.
- Goudriaan, J., H. H. Van Laar, H. Van Keulen, W. Louwerse, (1985), Photosynthesis, CO₂ and plant production. In: Day, W., Atkin, R.K. (Eds.), *Wheat Growth and Modelling. NATO ASI Series, Series A: Life Sciences*, **86**, pp. 107–122.
- Goudriaan, J., (1986), A simple and fast numerical method for the computation of daily totals of crop photosynthesis. *Agric. For. Meteorol.*, **38**, 249-254.
- Jacobs, C. M. J., (1994), Direct impact of atmospheric CO₂ enrichment on regional transpiration. PhD thesis, Wageningen Agricultural University.
- Jacobs, C.M.J., B.J.J.M. van den Hurk and H.A.R. de Bruin, (1996), Stomatal behaviour and photosynthetic rate of unstressed grapevines in semi-arid conditions. *Agric. For. Meteorol.*, **80**, 111-134.

- Jarvis, P. J., (1976), The interpretation of the variations in leaf-water potential and stomatal conductance found in canopies in the field, *Phil. Trans. of the Roy. Soc. London*, **B723**, 385-610.
- Knorr, W., N. Gobron, M. Scholze, T. Kaminski, R. Schnur, B. Pinty, (2007), Impact of terrestrial biosphere carbon exchanges on the anomalous CO₂ increase in 2002-2003, *Geophys. Res. Lett.*, **34**, L09703, doi: 10.1029/2006GL029019.
- Koster, R. D., S. Mahanama, T. Yamada, G. Balsamo, M. Boisserie, P. Dirmeyer, F. Doblas-Reyes, T. Gordon, Z. Guo, J.-H. Jeong, D. Lawrence, Z. Li, L. Luo, S. Malyshev, W. Merryfield, S. I. Seneviratne, T. Stanelle, B. van den Hurk, F. Vitart, E. F. Wood, (2010), The Contribution of Land Surface Initialization to Subseasonal Forecast Skill: First Results from the GLACE-2 Project, *Geophys. Res. Lett.*, **37**, L02402, doi:10.1029/2009GL041677.
- Lafleur, P.M., N.T. Roulet, J.L. Bubier, T.R. Moore and S. Frolking, (2003), Interannual variability in the peatland-atmosphere carbon dioxide exchange at an ombrotrophic bog. *Glob. Biogeochem. Cyc.*, **17**(2), 5.1-5.13, 1036, doi:10.1029/2002GB001983.
- Loveland, T. R., B. C. Reed, J. F. Brown, D. O. Ohlen, Z. Zhu, L. Youing, and J. W. Merchant, (2000), Development of a global land cover characteristics database and IGB6 DISCover from the 1km AVHRR data. *Int. J. Rem. Sens.*, **21**, 1303–1330.
- Le Quéré, C., M. R. Raupach, J. G. Canadell, G. Marland, et al., (2009), Trends in the sources and sinks of carbon dioxide. *Nature Geoscience* **2**, 831 - 836.doi:10.1038/ngeo689.
- Ma, S., D. D. Baldocchi, L. Xu and T. Hehn, (2007), Inter-annual variability in carbon dioxide exchange of an oak/grass savanna and open grassland in California. *Agri. For. Meteorol.*, **147**, 157-171
- Masson, V., J.L. Champeaux, F. Chauvin, C. Mériguet and R. Lacaze, (2003), A global database of land surface parameters at 1km resolution for use in meteorological and climate models. *J. Climate*, **16**, 1261-1282.
- McGuire A.D., J.M. Melillo, L.A. Joyce, D.W. Kicklighter, A.L. Grace, B. Moore III and C.J. Vorosmarty, (1992), Interactions between carbon and nitrogen dynamics in estimating net primary productivity for potential vegetation in North America., *Glob. Biogeochem. Cyc.*, **6**, 2, 101-124.
- Mkhabela, M.S., B.D. Amiro, A.G. Barr, T.A. Black, I. Hawthorne, J. Kidston, J.H. McCaughey, A.L. Orchansky, Z. Nesic, A. Sass, A. Shashkov and T. Zha, (2009), Comparison of carbon dynamics and water use efficiency following fire and harvesting in Canadian boreal forests. *Agri. For. Meteorol.*, **149**, 783-794.
- Myneni, R. B., R. R. Nemani, S. W. Running, (1997), Estimation of global leaf area index and absorbed PAR using radiative transfer models, *IEEE Trans. Geosc. Rem. Sensing*, **35**, no. 6.
- Olivier, J. G. J. and J. Berdowski, (2001), Global emissions, sources and sinks, in *The Climate System*, edited by J. Berdowski, R. Guicherit, and B. Heij, pp. 33– 78, A. A. Balkema, Lisse, Netherlands.

- Potter, C. S., J. T. Randerson, C. B. Field, P. A. Matson, P. M. Vitousek, H. A. Mooney, and S. A. Klooster, (1993), Terrestrial ecosystem production: A process model based on global satellite and surface data, *Glob. Biogeochem. Cyc.*, **7**(4):811-841.
- Reichstein, M., E. Falge, D. Baldocchi, D. Pappalardo, M. Aubinet, P. Berbigier, C. Bernhofer, N. Buchmann, T. Gilmanov, A. Granier, T. Grunwald, K. Havrankova, H. Ilvesniemi, D. Janous, A. Knohl, T. Laurila, A. Lohila, D. Loustau, G. Matteucci, T. Meyers, F. Miglietta, J.-M. Ourcival, J. Pumpanen, S. Rambal, E. Rotenberg, M. Sanz, J. Tenhunen, G. Seufert, F. Vaccari, T. Vesala, D. Yaki and R. Valentini, (2005), On the separation of net ecosystem exchange into assimilation and ecosystem respiration: review and improved algorithm. *Global Change Biology*, **11**, 1424–1439.
- Ronda, R.J., H. A. R. De Bruin, A. A. M. Holtslag, (2001), Representation of the canopy conductance in modelling the surface energy budget for low vegetation. *J. Appl. Meteorol.* **40**, 1431–1444.
- Roujean, J.-L., 1996. A tractable physical model of shortwave radiation interception by vegetative canopies. *J. Geophys. Res.* **101**(D5), 9523-9532.
- Sala, A. and J. Tenhunen, (1996), Simulations of canopy net photosynthesis and transpiration in *Quercus ilex* L. under the influence of seasonal drought. *Agri. For. Meteorol.* **78**, 203 - 222.
- Simmons, A. J., K. M. Willett, P.D. Jones, P. W. Thorne, D. P. Dee, (2010), Low-frequency variations in surface atmospheric humidity, temperature, and precipitation: Inferences from reanalyses and monthly gridded observational data sets. *J. Geophys. Res.* **115**: D01110, DOI: 10.1029/2009JD012442.
- Sitch, S., C. Huntingford, N. Gedney, P. E. Levy, M. Loma , S. L. Piao, R. Betts, P. Ciais , P. Cox, P. Friedlingstein , C. D. Jones, I. C. Prentice and F. I. Woodward, (2008), Evaluation of the terrestrial carbon cycle, future plant geography and climate-carbon cycle feedbacks using five Dynamic Global Vegetation Models (DGVMs). *Global Change Biology*, **14**, 1-25, doi: 10.1111/j.1365-2486.2008.01626.x
- Szczypta, C., J.-C. Calvet, C. Albergel, G. Balsamo, S. Boussetta, D. Carrer, S. Lafont, and C. Meurey, (2011), Verification of the new ECMWF ERA-Interim reanalysis over France, *Hydrol. Earth Syst. Sci.*, **15**, 647-666, doi:10.5194/hess-15-647-2011.
- Takahashi, T., S. C. Sutherland, R. Wanninkhof, C. Sweeney, R. A. Feely, D. W. Chipman, B. Hales, G. Friederich, F. Chavez, A. Watson, D. C. E. Bakker, U. Schuster, N. Metzl, H. Yoshikawa-Inoue, M. Ishii, T. Midorikawa, Y. Nojiri, C. Sabine, J. Olafsson, T. S. Arnarson, B. Tilbrook, T. Johannessen, A. Olsen, R . Bellerby, A. Körtzinger, T. Steinhoff, M. Hoppema, H. J. W. de Baar, C. S. Wong, B. Delille, N. R. Bates, (2009), Climatological mean and decadal changes in surface ocean pCO₂, and net sea-air CO₂ flux over the global oceans. *Deep-Sea Res. II*, **56**, 554-577.
- Van den Hurk, B. J. J. M., P. Viterbo, A. C. M. Beljaars, and A. K. Betts, (2000), Offline validation of the ERA-40 surface scheme. *ECMWF Tech. Memo.* No. **295**.

- Van den Hurk, B. and P. Viterbo, (2003a), The Torne-Kalix PILPS 2(e) experiment as a test bed for modifications to the ECMWF land surface scheme. *Global and Planetary Change*, **38**, 165–173.
- Van den Hurk, B.J.J.M., P. Viterbo and S. O. Los, (2003b), Impact of Leaf area index seasonality on the annual land surface evaporation in a global circulation model, *J. Geophys. Res.*, **108**, N0 D6, 4191, doi:10.1029/2002JD002846.
- Van der Werf, G. R., J. T. Randerson, L. Giglio, G. J. Collatz, M. Mu, P. S. Kasibhatla, D. C. Morton, R. S. DeFries, Y. Jin, and T. T. van Leeuwen, (2010), Global fire emissions and the contribution of deforestation, savanna, forest, agricultural, and peat fires (1997-2009), *Atmos. Chem. Phys.*, **10**, doi:10.5194/acp-10-11707-2010.
- Viterbo P. and A.C.M. Beljaars, (1995), An improved land surface parametrization scheme in the ECMWF model and its validation, *ECMWF Technical Report*, **75**, Reading, UK.
- Viterbo P., A.C.M. Beljaars, J.-F. Mahouf, J. Teixeira, (1999), The representation of soil moisture freezing and its impact on the stable boundary layer. *Q. J. R. Meteorol. Soc.* **125**, 2401–2426.
- Voogt, M.H., B.J.J.M. van den Hurk and C.M.J. Jacobs, (2006), The ECMWF land-surface scheme extended with a photosynthesis and LAI module tested for a coniferous site. *KNMI Scientific Report*, WR 2006-02. Available from KNMI, De Bilt.
- White, M.A., P.E. Thornton, S.W. Running and R.R. Nemani, (2000), Parameterization and sensitivity analysis of the BIOME-BGC terrestrial ecosystem model: net primary production controls, *Earth Interactions*, **4** (3), 1-84.
- Wohlfahrt, G., A. Hammerle, A. Haslwanter, M. Bahn, U. Tappeiner, A. Cernusca, (2008), Seasonal and inter-annual variability of the net ecosystem CO₂ exchange of a temperate mountain grassland: effects of weather and management. *J. Geophys. Res.*, **113**, D08110, doi:10.1029/2007JD009286.
- Zhao, M., S. W. Running, and R. R. Nemani, (2006), Sensitivity of Moderate Resolution Imaging Spectroradiometer (MODIS) terrestrial primary production to the accuracy of meteorological reanalyses, *J. Geophys. Res.*, **111**, G01002, doi:10.1029/2004JG000004.